NACA

RESEARCH MEMORANDUM

A TRANSONIC WIND-TUNNEL INVESTIGATION OF THE EFFECTS OF

NACELLE SHAPE AND POSITION ON THE AERODYNAMIC

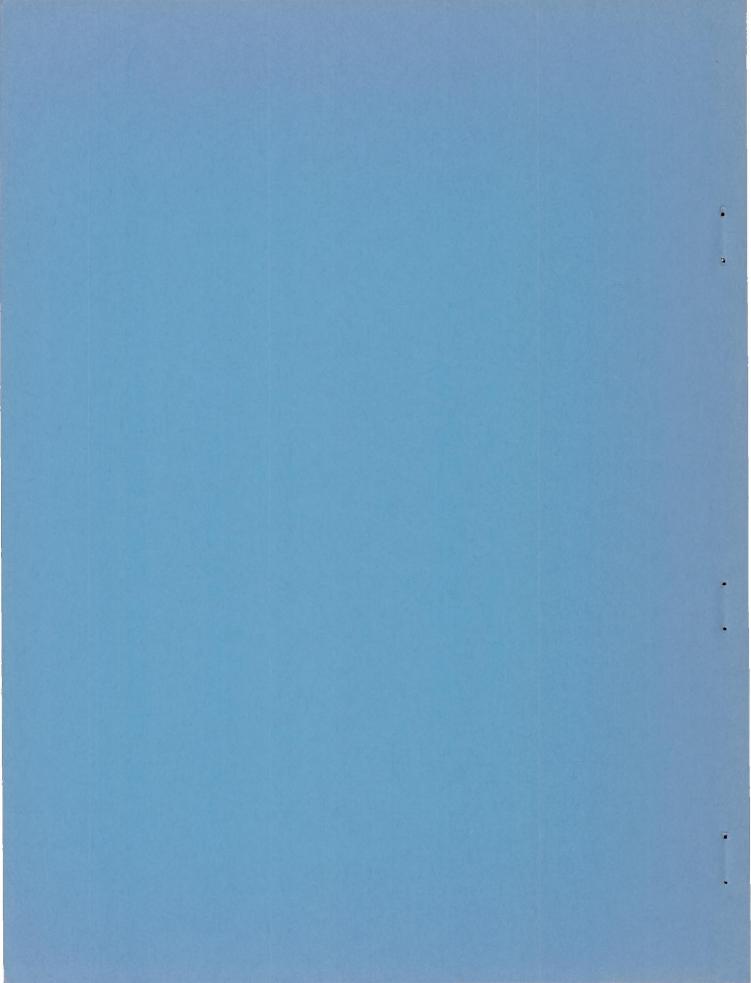CHARACTERISTICS OF TWO 47° SWEPTBACK

WING-BODY CONFIGURATIONS

By Ralph P. Bielat and Daniel E. Harrison

Langley Aeronautical Laboratory
Langley Field, Va.

NATIONAL ADVISORY COMMITTEE
FOR AERONAUTICS
WASHINGTON

September 2, 1952
Declassified August 14, 1958

NATIONAL ADVISORY COMMITTEE FOR AERONAUTICS

———————

RESEARCH MEMORANDUM

———————

A TRANSONIC WIND-TUNNEL INVESTIGATION OF THE EFFECTS OF

NACELLE SHAPE AND POSITION ON THE AERODYNAMIC

CHARACTERISTICS OF TWO 47° SWEPTBACK

WING-BODY CONFIGURATIONS

By Ralph P. Bielat and Daniel E. Harrison

SUMMARY

An investigation has been made in the Langley 8-foot transonic tunnel to determine the effects of nacelle shape and position on the aerodynamic characteristics of two wing-body configurations at Mach numbers varying from 0.50 to 1.12. The two wings had 47° sweepback of the 0.25-chord line, aspect ratio of 3.5, taper ratio of 0.2, and zero twist and dihedral. One configuration had a wing with constant streamwise thickness of 6 percent along the span; the other configuration employed a wing with 6-percent-thick sections outboard of the 40-percent-semispan station but tapered to a 12-percent-thick section at the plane of symmetry. Nacelles investigated consisted of underslung and pylon-suspended nacelles located at the 40-percent-semispan station, submerged nacelles, and wing-tip nacelles. Lift, drag, and pitching-moment coefficients were determined from strain-gage measurements. The Reynolds number of the tests based on the wing mean aerodynamic chord varied from 2.0×10^6 to 2.6×10^6.

The drag at high subsonic Mach numbers for the various nacelle configurations with the exception of the underslung and wing-tip nacelles was high when compared with the drag of the isolated nacelles. At transonic Mach numbers, the interference drag of the various nacelle configurations was high in nearly all cases. In general, configurations with the highest drag were those in which the maximum area of the nacelles occurred at or near the maximum cross-sectional area of the wing-body combination.

In the case of the nacelles located at the 40-percent-semispan station, moving the nacelles a moderate amount ahead of and down from the local wing chord caused substantial reductions in transonic

interference drag. Further chordwise and vertical movement did not
result in any appreciable drag reductions but had a favorable effect
on the drag-break Mach number. At Mach numbers up to about 0.80, the
strut and strut-end junctures of the pylon-suspended nacelles appeared
to be responsible for a large interference drag.

Moderate thickening of the wing root was accomplished without
penalty in minimum drag or maximum lift-drag ratio when the nacelles
were submerged in the wing root aft of the maximum-thickness station.
At high Mach numbers the wing-tip nacelles had the lowest incremental
drag coefficients and the highest maximum lift-drag ratio values of the
various nacelles investigated on the 6-percent-thick wing-body
configuration.

In general, the various nacelle configurations caused small
reductions in the drag-break Mach number and produced small increases
in the lift-curve-slope characteristics of the basic models. The pylon-
suspended and underslung nacelles produced destabilizing moments, whereas
the submerged and wing-tip nacelles caused stabilizing moments of the
basic models.

INTRODUCTION

The NACA has been conducting a broad program of research to
determine the aerodynamic characteristics at supersonic speeds
(refs. 1 to 3) and at transonic speeds (refs. 4 and 5) of wings varying
in thickness ratio and in sweep for use on a high-speed bomber. The
present paper presents the results at high-subsonic and transonic
speeds of a nacelle investigation conducted on two wing-body combinations
of this series. The wings both had 47° sweepback based on the 0.25-chord
line, aspect ratio 3.5, and taper ratio 0.2, but differed in root-section
configuration. Underslung, pylon-suspended, and wing-tip nacelles were
investigated in conjunction with one of these wings which had 6-percent-
thick sections throughout. Nacelles submerged in the wing root also
were studied on this wing and on the second wing which had a root section
that varied linearly in thickness ratio from 12 percent at the plane of
symmetry to 6 percent of the 40-percent-semispan station. The underslung
and pylon-suspended nacelles investigated on the 6-percent-thick wing
formed a consistent family in which forward movement of the nacelles
was accomplished by proportional downward movement so that the trailing
edge of the wing always cleared a 30°-included-angle conical surface
extending aft from the nacelle exit.

The results reported herein consist of lift, drag, and pitching-
moment measurements for a Mach number range of 0.50 to approximately 1.12.

In general, measurements were made for the nacelles in the faired and unducted condition; however, one nacelle configuration was provided with an internal ducting system which permitted a study of the external effects of internal air flow and of inlet and exit geometry. Total-pressure and static-pressure measurements were taken at the exit of the ducted nacelle to determine the mass flow, inlet-velocity ratio, and internal drag coefficient. The tests were conducted in the Langley 8-foot transonic tunnel.

SYMBOLS

A	area, sq ft
$\bar{c}$	mean aerodynamic chord of wing, in.
c'	point mass-flow coefficient, $\dfrac{\rho V}{\rho_o V_o}$
C_D	drag coefficient, D/qS
$C_{D_{int}}$	internal drag coefficient of flow nacelles based on wing area
ΔC_D	nacelle drag increment, drag-coefficient rise due to addition of nacelles to basic wing-body configuration; the factor used to convert the nacelle drag increment to a value based on nacelle frontal area is 46.57 for all nacelles
C_L	lift coefficient, L/qS
C_{L_α}	lift-curve slope per degree, $\dfrac{dC_L}{d\alpha}$
C_m	pitching-moment coefficient, $\dfrac{M_{\bar{c}/4}}{qS\bar{c}}$
D	drag, lb
L	lift, lb
$(L/D)_{max}$	maximum lift-drag ratio
m	mass-flow rate, ρAV, slugs/sec
M	Mach number

M_B drag-break Mach number defined as value where $\dfrac{dC_D}{dM} = 0.10$

$M_{\overline{c}/4}$ pitching moment of aerodynamic forces about lateral axis which passes through 25-percent point of mean aero-dynamic chord of wing, inch-pounds

q dynamic pressure, $\dfrac{1}{2}\rho_o V_o^2$, lb/sq ft

r radius, measured from nacelle center line, in.

R maximum radius of nacelle, in.

R Reynolds number based on $\overline{c}$

S wing area, sq ft

V velocity, fps

α angle of attack of body center line, deg

ρ air density, slugs/cu ft

Subscripts:

o   free stream

1   nose-inlet entrance

APPARATUS AND METHODS

Tunnel

The tests were conducted in the Langley 8-foot transonic tunnel which is a dodecagonal, slotted-throat, single-return type of wind tunnel. The use of longitudinal slots along the test section permitted the testing of the models through the speed of sound without the usual choking effects found in the conventional closed-throat type of wind tunnel. Typical Mach number distributions along the center of the slotted test section are shown in figure 1. Local deviations from the average free-stream Mach number in the region of the model were no larger than 0.003 at subsonic speeds. With increases in Mach number above 1.00, the deviations increased but did not exceed 0.010 at a Mach number of 1.13. A complete description of the Langley 8-foot transonic tunnel can be found in reference 6.

Model

Wing-body configuration.- The models employed for the tests were
supplied by a U. S. Air Force contractor and were constructed of steel.
The two basic wing-body combinations were midwing configurations and
as shown in figure 2 had wings of 47° sweepback of the 0.25-chord line,
aspect ratio of 3.5, taper ratio of 0.2, zero twist and dihedral, and
the following airfoil section parallel to the model plane of symmetry:

Thickness distribution . . . . NACA 65A-series
Mean-line ordinates . . . . .1/3 of NACA 230 series plus NACA
                                        6-series uniform-load mean line
                                        (a = 1.0) for a design lift
                                        coefficient of 0.1

The wing of one of the models had a constant streamwise thickness
of 6 percent along the span W_1, and the other model employed a wing
with 6-percent-thick sections outboard of the 40-percent-semispan
station but tapered to a 12-percent-thick section at the plane of
symmetry W_2. Airfoil coordinates for the two wings are given in
table I. The body was a steel shell with an ogival nose followed by
a constant-diameter cylindrical section with a ratio of body diameter
to wing span of about 0.094.

Underslung and pylon-suspended nacelles.- The underslung and pylon-
suspended nacelles were bodies of fineness ratio 9.51 formed by adding
ogival nose and tail sections to a cylindrical midsection. The under-
slung nacelles, designated as N_u herein, were attached to the 6-percent-
thick wing W_1 at the 0.40-semispan station such that the upper surface
of the nacelles was tangent to the wing-chord plane. The pylon-suspended
nacelles were attached to the same wing at the same spanwise station by
means of 75° sweptforward struts which had a thickness ratio of 5 percent
parallel to the free stream. Three chordwise positions, N_1, N_2, and N_3
were studied by progressively lengthening the support strut. Since the
forward movement of the nacelle was accompanied by a proportional
downward movement, the underslung and pylon-suspended nacelles formed
a consistent family in which the trailing edge of the wing always just
cleared a 30°-included-angle conical surface extending aft from the
nacelle exit. The nacelle and strut details are given in figures 3
and 4. The designations given the various nacelle positions in figure 3
are used throughout this paper.

Pylon-suspended nacelles with air flow.- The pylon-suspended
nacelle N_2 was modified to permit internal air flow by the provision
of a 1.0-inch-diameter cylindrical duct through the body (figs. 4 and 5).

As shown in figure 5, NACA 1-series nose-inlet ordinates were used in both nose and tail fairings, and several different nose and tail shapes were investigated in order to determine the major effects of the proportions of these components. The designations given the ducted nacelles in figure 5 are used to identify the configurations throughout this paper.

Submerged nacelles.- The submerged nacelles were tested with both the 6-percent-thick and the thickened-root wing models W_1 and W_2. The submerged nacelles consisted of two nacelles on each wing semispan located slightly below the wing-chord plane and rearward of the wing maximum thickness at the 0.141- and 0.234-semispan stations. The submerged nacelles on the 6-percent-thick wing were designed to have scoop-type inlets, whereas the submerged nacelles on the thickened-root wing were designed to have wing-leading-edge inlets. The internal ducting for the submerged nacelles, however, was not simulated for the present tests. The frontal areas of the submerged nacelles and of the pylon-suspended nacelles were equal. A photograph of the submerged nacelles on the thickened-root wing-body configuration is shown in figure 6 and details of the nacelles are given in figure 7. The submerged nacelles on the 6-percent-thick wing and on the thickened-root wing have been designated as N_{s1} and N_{s2}, respectively.

Wing-tip nacelles.- The wing-tip nacelles had the same dimensions as the pylon-suspended nacelles. The wing-tip nacelles were mounted symmetrically with respect to the wing-chord plane on the 6-percent-thick wing as shown in figure 8. The designation N_{wt} has been given the wing-tip nacelles in the present paper.

Model Support System

The models were attached to the sting support through a six-component, internal, electrical strain-gage balance which was provided by a U. S. Air Force contractor. Angle-of-attack changes of the models were accomplished by pivoting the sting about a point which was located approximately 66 inches downstream of the 0.25-mean-aerodynamic-chord point. A sting bent 15° ahead of the pivot point was used in order to keep the model position reasonably close to the tunnel axis when the model angle of attack was varied from 6° to 12°. The angle mechanism was controlled from outside the test section and therefore permitted angle changes with the tunnel operating. A detailed description of the support system can be found in reference 7.

Measurements

Lift, drag, and pitching moment were determined by means of an electrical strain-gage balance located inside the body. For the basic models, measurements were taken for angles of attack from -2° to 14° at Mach numbers varying from 0.50 to approximately 0.95 and from -2° to 6° at Mach numbers varying from 1.00 to approximately 1.12. In general, the models with the nacelles were tested for angles of attack from -2° to 7°. The accuracy of the data at a Mach number of 0.50, based on the static calibration of the balance and the reproducibility of the data, is as follows:

C_L . . . . ±0.005
C_D . . . .±0.0005
C_m . . . . ±0.004

The accuracy of the data is improved at the higher Mach numbers.

A pendulum-type accelerometer, calibrated against angle of attack and located within the sting downstream of the model, was used to indicate the angles of the model relative to the air stream. For actual testing conditions, however, it was necessary to apply a correction to the angle of attack of the model caused by the elasticity of the sting-support system.

The use of the calibrated accelerometer in conjunction with the remotely controlled angle-of-attack changing mechanism allowed the model angle to be set within ±0.1° for all test Mach numbers.

Reynolds Number

The variation of test Reynolds number, based on the mean aerodynamic chord of the wing, with Mach number averaged for several runs is presented in figure 9. The Reynolds number varied from 2.0×10^6 to 2.6×10^6 for the present investigation.

Corrections

The usual corrections to the Mach number and dynamic pressure for the effects of the model and wake blockage and to the drag coefficient for the effect of the pressure gradient caused by the wake are no longer necessary with the use of longitudinal slots in the test section (ref. 8). The data reported herein have been corrected for a slight misalinement of the tunnel air stream.

The drag data have been corrected for base pressure such that the drag corresponds to conditions where the body base pressure is equal to the free-stream static pressure.

No correction for wing twist due to bending of the swept wings has been applied to the data. Calculations using theoretical span loadings given in reference 9 and the stiffness properties of the wings indicated that bending had a negligible effect on the data presented herein.

There exists a range of Mach numbers above Mach number 1.0 where slotted-tunnel data are affected by reflected shock waves. On the basis of the results of reference 10, it was estimated that the reflected nose shock wave should clear the rear of the model at Mach numbers above 1.08. Schlieren pictures made during the present tests substantiated these calculations. The results of reference 10 also indicate that although a detached bow wave exists ahead of the model at low supersonic Mach numbers the reflected wave up to a Mach number of approximately 1.04 is of such weak intensity that the data are not appreciably affected. Accordingly, no data were taken in the range of Mach numbers from 1.04 to 1.08, and in the final cross plots of the results the curves are faired in this range of Mach numbers.

RESULTS

An index of the figures presenting the results is as follows:

Type of plot	Figure number for -					
	Basic model W_1	Basic model W_2	Underslung and pylon-suspended nacelles N_u, N_1, N_2, N_3	Submerged nacelles N_{s1}, N_{s2}	Wing-tip nacelles N_{wt}	Pylon-suspended nacelles with air flow N_{2a}, N_{2b}, N_{2c}, N_{2d}
α, C_D, C_m against C_L	10	11	12 to 15	16, 17	18	19 to 22
ΔC_D against M			23	29	32	26
$(L/D)_{max}$ against M	24, 27 30, 33	30	24	30	33	27
M_B against C_L	25, 28 31, 34	31	25	31	34	28
c' against $(r/R)^2$						35
$C_{D_{int}}$ against C_L						36
$m/\rho_o V_o A_1$ against M						37
V_1/V_o against M						38
Schlieren photographs						39
C_{L_α} against M	40	40	40(a)	40(b)	40(c)	40(d)
Aerodynamic-center location against M	41	41	41(a)	41(b)	41(c)	41(d)

The reference axes of the data presented in the figures have been changed from body axes to wind axes. In order to facilitate presentation of the data, staggered scales have been used in many of the figures and care should be taken in identifying the zero axis for each curve.

DISCUSSION

A summary of the aerodynamic characteristics of the various nacelle configurations tested on the 6-percent-thick wing-body configuration is given in table II. The transonic interference drag of the nacelles was high in nearly all cases. In general, the configurations with highest drag were those in which the maximum area of the nacelles occurred at or near the maximum cross-sectional area of the wing-body combination. In this respect, therefore, the requirement for avoiding large transonic interference drag is similar to that for delaying compressibility effects at subsonic speeds; namely, the addition of points of maximum thickness or peak negative pressures should be avoided.

Drag Characteristics

Underslung and pylon-suspended nacelles.- The effects of changes in nacelle location at the 40-percent-semispan wing station on the incremental drag coefficients of the nacelles for 0 and 0.3 lift coefficients are presented in figure 23. There is also included in figure 23 the drag coefficient for two isolated nacelles as determined from unpublished rocket data. These values were based on the wing area of the present model. A comparison between the drag of the isolated nacelles and the measured nacelle drag is indicative of the level of the interference drag. Up to a Mach number of 0.80 and at zero lift coefficient, the underslung nacelles N_u had the lowest incremental drag of this group of nacelles. The fact that the incremental drag for these underslung nacelles was lower than that for the isolated nacelles indicates the existence of favorable interference effects in this range of Mach number.

At zero lift coefficient and up to a Mach number of 0.80, the incremental drag coefficients for the pylon-suspended nacelles N_1, N_2, and N_3 were all approximately 50 percent higher than those for the isolated nacelles. The reason for this large subsonic interference drag is not understood. The fact that it did not change appreciably with changes in nacelle position, however, seems to indicate that it was caused mainly by the struts or the strut end junctures rather than by the nacelles.

At transonic Mach numbers, important differences in the incremental drag values were noted as the nacelles were moved forward and downward from position N_u to position N_3. At a Mach number of 1.00, the interference drag of the pylon-suspended nacelles in position N_1 was the same as that for the underslung nacelles N_u and was approximately twice the drag of the isolated nacelles; in position N_2 the interference drag was about equal to the drag of the isolated nacelles; and in position N_3 there was little or no interference drag, that is, the measured nacelle drag was approximately equal to the drag of the isolated nacelles. Unfortunately, sufficient schlieren photographs were not obtained in the transonic speed range to determine the nature of the changes in the flow phenomena responsible for these changes in the interference drag; the complexities of the air flow, especially near $M = 1.00$, can be observed in the schlieren photographs shown in figure 39 for the pylon-suspended nacelles with air flow in position N_2. At a Mach number of 1.10, a change in nacelle position from N_u or N_1 to N_2 caused a marked reduction in the interference drag, but further movement of the nacelles to position N_3 produced negligible further change. The transonic interference drags of nacelles N_2 and N_3, although much lower than those of N_u and N_1, were still of important magnitude.

The results at a lift coefficient of 0.3, figure 23, show that the nacelles with the shortest pylon length N_1 produced much larger interference drag values at Mach numbers up to 1.00 than nacelles N_u, N_2, and N_3. The high level of the subsonic incremental drag for this nacelle could be due to its poor chordwise and vertical location (similar results are reported in ref. 11). At a Mach number of 1.00, large reductions in the incremental drag coefficients again occurred as the nacelles were moved forward and down from position N_1 to position N_3. At a Mach number of 1.10, the incremental drag coefficients of nacelles N_2 and N_3 again were about equal and very much lower than those for N_u and N_1.

Maximum lift-drag ratios for model W_1 with and without the nacelles just discussed are presented in figure 24. As would be expected on the basis of the data for $C_L = 0.3$ in figure 23, the maximum lift-drag ratios at subsonic speeds for the model with nacelles N_u, N_2, and N_3 were approximately equal and were significantly greater than those for nacelle configuration N_1. As also would be expected, nacelle configurations N_2 and N_3 were markedly superior to N_u and N_1 at supersonic speeds.

The variations of drag-break Mach number with lift coefficient for the basic model and for the underslung nacelles and the pylon-suspended nacelles are presented in figure 25. The drag-break Mach number is defined in this paper as the value where $\frac{dC_D}{dM} = 0.10$. The underslung nacelles and the pylon-suspended nacelles in positions N_1 and N_2 reduced the drag-break Mach number of the basic configuration approximately 0.030 for a lift-coefficient range from 0 to 0.35. Moving the nacelles further from the wing reduced the adverse effects of the nacelle; nacelle configuration N_3 did not cause any measurable reduction in drag-break Mach number above a lift coefficient of 0.26.

Pylon-suspended nacelles with air flow.- The variations of incremental drag coefficient with Mach number for the pylon-suspended nacelles with air flow in position N_2 for 0 and 0.3 lift coefficients are shown in figure 26. Modifications were made to these ducted nacelles in order to show the effects of the shapes and locations of the inlets and exits. The incremental drag coefficients were based upon the wing area and include the internal drag of the nacelles. Flow measurements were made for nacelles N_{2a} in order to determine the mass flow and internal drag characteristics. The results of these measurements are given in figures 35 to 38. It will be noted that the internal drag of the nacelles is small and, therefore, would have a negligible effect on the incremental drag values. The ducted nacelles generally had appreciably higher incremental drag coefficients than the faired nacelles N_2 except in a limited region near $M = 1.00$. This difference in drag could be attributed to the increased bluntness of the body (inlets and exits) compared with the basic body. Results presented in reference 12 indicate that the drag difference should be negligible provided the inlet and exit shapes were comparable with those for the faired nacelles. It will also be noted that the differences in the incremental drag values for the various ducted nacelles generally are small.

Maximum lift-drag ratios for the various ducted nacelles in position N_2 are given in figure 27. With the exception of N_{2a} at subsonic speeds, all of the ducted nacelle configurations had approximately equal maximum lift-drag ratios throughout the test Mach number range. Nacelle N_{2a} was appreciably superior to the other nacelles with regard to maximum lift-drag ratios for subsonic Mach numbers up to about 0.92.

The drag-break Mach number of the basic 6-percent-thick wing model, as indicated in figure 28, was reduced approximately 0.03 to 0.05 in

Mach number due to the addition of the various ducted nacelle configurations. Again, a better nacelle shape might have reduced this penalty.

Submerged nacelles.- The variation of incremental drag coefficient with Mach number for the submerged nacelle installations, N_{s1} and N_{s2}, is shown in figure 29. At zero lift coefficient, the submerged nacelles N_{s1} increased the drag of the model with the 6-percent-thick wing from 11 percent at a Mach number of 0.70 to 39 percent at a Mach number of 1.10. On the other hand, the submerged nacelles N_{s2} caused a 38-percent increase in the drag of the thickened wing-root model at a Mach number of 0.70 and only a 12-percent increase in the drag at a Mach number of 1.10. The reason for the difference in drag levels at subsonic Mach numbers for the two submerged nacelles is due to the lower drag values at zero lift of the thickened-root wing model as compared with the 6-percent-thick wing model. The drag coefficients at zero lift for the two basic wing models are also included in figure 29.

Because of the differences in the drag coefficients of the basic models, the total drag coefficients for the two submerged nacelle configurations are of greater significance than the incremental drag coefficients. A comparison of the data of figures 16 and 17 shows that the minimum drags of the two configurations were very nearly the same throughout the test Mach number range. This result is particularly significant at supersonic Mach numbers near 1.10 where the minimum drag of the basic 6-percent-thick wing model W_1 was about 20 percent lower than that of thickened-wing-root model W_2.

Maximum lift-drag ratios for the basic and submerged-nacelle models are presented in figure 30. The maximum lift-drag ratios for the submerged nacelle model with the thickened wing root N_{s2} were slightly higher than those for the submerged nacelle model with the 6-percent-thick wing N_{s1} for Mach numbers up to about 0.95 and were approximately equal to the values for this model at all higher test Mach numbers. Moderate thickening of the wing root (the difference between models W_1 and W_2) was therefore accomplished without penalty in drag or lift-drag ratio when the nacelles were located in the wing root rearward of the maximum thickness station.

The results presented in figure 31 show that the submerged nacelles N_{s1} reduced the drag-break Mach number of the 6-percent-thick wing model approximately 3 percent whereas the submerged nacelles N_{s2} generally had a negligible effect on the drag-break Mach number of the thickened-root-wing model.

Wing-tip nacelles.- The variations of the incremental drag coefficients with Mach number at 0 and 0.3 lift coefficients for the wing-tip nacelles

are shown in figure 32. The drag coefficient for the isolated nacelles obtained from unpublished rocket data is also included in figure 32. Of the various nacelle configurations tested on the 6-percent-thick wing model, the nacelles located at the wing tips had the smallest transonic drag rise for both 0 and 0.3 lift coefficients; however, the drag level generally was still high when compared to that of the isolated nacelles. At zero lift coefficient and a Mach number of 1.10, the drag of the basic model was increased about 29 percent by the addition of the wing-tip nacelles whereas the pylon-suspended nacelles in positions N_2 and N_3 and the submerged nacelles N_{s1} increased the drag of the basic model by approximately 39 percent. A comparison of the incremental drag coefficients with the drag of the isolated nacelles for zero lift coefficient and a Mach number of 1.10 indicated that the interference drag for the pylon-suspended nacelles in positions N_2 and N_3 was approximately twice that of the wing-tip nacelles. The lower drag values for the wing-tip nacelle installation at the high Mach numbers are believed to be due to a reduction in the severity of the adverse interference effects as a result of the complex flow fields that exist at transonic speeds as discussed in reference 13.

Although the discussion of the flow phenomena in reference 13 is for a wing-fuselage combination having a wing of aspect ratio 4.0, taper ratio 0.6, 45° sweptback of the 0.25-chord line, and NACA 65A006 airfoil sections parallel to the plane of symmetry, it is believed that similar phenomena exist for the wing-body configuration of the present investigation. The following discussion is a brief résumé of the results reported in reference 13. At Mach numbers approaching 1.00, there is a strong normal shock over the wing which extends laterally beyond the wing tips. For the present model, this shock would pass over the wing-tip nacelle at approximately 70 percent of its length. A strong normal shock also emanates from the fuselage behind the wing trailing edge and merges with the wing normal shock near the wing tip. As the Mach number was increased to values above 1.00, the fuselage shock separates from the wing shock and moves downstream of the wing tip. Strong oblique shocks from the wing-fuselage leading-edge intersection also develop at Mach numbers at and above 1.00 and extend laterally beyond the wing tips. It is believed that the resulting pressure rise through the shocks as the shocks act over the after portion of the nacelles could reduce the drag of the wing-tip nacelles provided the shocks did not cause separation of the flow over the nacelles.

The effects of the wing-tip nacelles on the variation of maximum lift-drag ratio with Mach number is presented in figure 33. The addition of the wing-tip nacelles to the basic model configuration caused a 19 percent reduction in the value of the maximum lift-drag ratio at a Mach number of 0.70 as compared to a decrease of about

21 percent for the pylon-suspended nacelles in positions N_2 and N_3 and to the submerged nacelles N_{s1}. At a Mach number of 1.10, the wing-tip nacelles decreased the $(L/D)_{max}$ value of the basic model from 9.0 to 7.9 or approximately 12 percent, whereas the pylon-suspended nacelles in positions N_2 and N_3 and the submerged nacelles (N_{s1}) lowered the the $(L/D)_{max}$ values of the basic model by about 19 percent. The higher $(L/D)_{max}$ values for the wing-tip nacelles could be expected since the incremental drag values at zero lift coefficient and the drag due to lift as indicated by the high values of lift-curve slope were lower than those for the other nacelle configurations tested on the 6-percent-thick wing.

The effects of the wing-tip nacelles on the drag-break Mach number of the basic model are presented in figure 34. The wing-tip nacelles reduced the drag-break Mach number of the basic model approximately 0.025 throughout the lift coefficient range shown.

Mass-Flow Characteristics

The results of the mass-flow measurements for the pylon-suspended nacelle N_{2a} are presented in figures 35 to 38. The variation of point mass-flow coefficient with area ratio (fig. 35) indicated, as to be expected, that as the angle of attack was increased, the air flow through the nacelle had a tendency to separate from the lower wall. It would also be expected that no separation of the air flow in the duct would be evident for 0° angle of attack for the Mach numbers shown. Separation of the air flow from the upper wall, however, was indicated at 0° angle of attack for Mach numbers 1.00 and 1.10. Separation of the flow from the lower wall that existed at 2° angle of attack for Mach numbers below 1.00, on the other hand, was not evident for Mach numbers of 1.00 and 1.10. It is believed that these characteristics are probably due to the turning of the entering air flow caused by the bow waves ahead of the body and of the nacelles (see fig. 39) and to the sharp nose radius of the nacelles.

The internal drag characteristics of the nacelle are presented in figure 36. The internal drag coefficient was based upon the wing area and represents the internal drag of only one nacelle. It can be seen that the effects of compressibility on the internal drag coefficient are negligible. It should be stated that a normal shock was evident downstream of the measuring station at the nacelle exit (fig. 39) and the losses through this shock were not included in the internal drag.

The variation of mass-flow ratio with Mach number for 0° angle of attack for the pylon-suspended nacelle is shown in figure 37. The mass-flow ratio increased from a value of 0.85 at a Mach number of 0.50 to 0.90 at a Mach number of 1.10.

The variation of inlet velocity ratio with Mach number for 0° angle of attack is given in figure 38. The inlet velocity ratio decreased from a value of 0.81 to 0.65 as the Mach number increased from 0.50 to 1.10.

Schlieren Photographs

Schlieren photographs of the flow over the body and nacelles at 0° angle of attack are shown in figure 39. Two disturbances in the flow are evident at a Mach number of 0.97. The disturbance "a" is a normal shock on the nacelle. Pressure distributions on a very nearly similar inlet (ref. 14) indicated a shock to form at approximately the same location shown in the photograph. The disturbance "b" is also a normal shock which occurred at the rearward end of the nacelle. Behind the normal shock "a" the flow essentially returned to free-stream velocity but as the flow approached the rearward end of the nacelle, it again expanded to local supersonic velocities due to the curvature of the nacelle exit. Since the flow through the nacelle was choked at the exit as indicated by the total-pressure and static-pressure measurements, the flow downstream of the exit expanded to supersonic speeds caused by the low pressures of the expanding flow around the rearward end of the nacelle and then terminated with the normal shock "b". An oblique shock extending from the normal shock "b" which turns the air flow parallel with the stream is also evident. With an increase in Mach number to 1.00, an additional disturbance "c" is formed which is due to the intersection of the nacelle strut and the leading edge of the wing at the 0.40-semispan station. At a Mach number of 1.024, a detached bow wave "d" is seen to approach the body and a detached wave "e" to approach the inlet of the nacelle. The disturbances "a" and "c" have become oblique to the flow. As the Mach number was increased to approximately 1.12, the various disturbances have become more pronounced and more oblique to the flow. The bow wave "d" now has become attached to the nose of the body. The normal shock "b" at the nacelle exit is still evident even though the free-stream velocity is supersonic.

Lift Characteristics

The effects of changes in the location of the various nacelles on the lift-curve slopes of the 6-percent-thick wing W_1 and the thickened-root wing W_2 are shown in figure 40. These curves represent average

slope values for the linear-lift range. The addition of the nacelles
generally increased the lift-curve slope values of the basic model.
Except for the wing-tip nacelles and Mach numbers near 0.95, these
increases in the lift-curve slopes were generally small. The rather
large increases in the lift-curve slopes for the wing-tip nacelles
could be due to the end-plate effect of the nacelles on the wing.

Longitudinal Stability Characteristics

The rate of change of pitching-moment coefficient with lift coef-
ficient (dC_m/dC_L) was obtained in order to determine the aerodynamic-
center location in percent of the mean aerodynamic chord of the various
model configurations. The slopes were averaged over the linear portion
of the curves and represent average values for a range from 0 to
approximately 0.3 lift coefficient. The effect of the various nacelle
configurations on the aerodynamic-center location is presented in
figure 41. The pylon-suspended nacelles with and without air flow and
the underslung nacelles produced destabilizing moments as indicated by
the forward shifts in the aerodynamic-center location when compared
with the basic model. The forward shifts in the aerodynamic-center
location amounted to approximately 2 to 5 percent of the mean aerodynamic
chord. The submerged nacelles and the wing-tip nacelles, on the other
hand, caused stabilizing moments of about 2 to 6 percent rearward shifts
in the aerodynamic-center location as compared with the basic models.
It is also evident that as the Mach number increased from 0.50 to 1.10,
the aerodynamic-center location of all configurations moved rearward
about 16 percent which compared with a similar rearward movement for
the basic models.

CONCLUSIONS

An investigation was made in the Langley 8-foot transonic tunnel
of the effects of nacelle shape and position on the aerodynamic charac-
teristics of two sweptback wing-body configurations. The two wings had
47° sweepback of the 0.25-chord line, aspect ratio of 3.5, taper ratio
of 0.2, and zero twist and dihedral. One configuration had a wing with
a constant streamwise thickness of 6 percent along the span. The other
configuration employed a wing with 6-percent-thick sections outboard
of the 40-percent-semispan station but tapered to a 12-percent-thick
section at the plane of symmetry. Nacelles investigated consisted of
underslung and pylon-suspended nacelles located at the 40-percent-
semispan station, submerged nacelles, and wing-tip nacelles. The fol-
lowing conclusions are indicated:

1. The drag at high-subsonic Mach numbers for the various nacelle configurations with the exception of the underslung and wing-tip nacelles was high when compared with the drag of the isolated nacelles. At transonic Mach numbers, the interference drag of the various nacelle configurations was high in nearly all cases. In general, the configurations with highest drag were those in which the maximum area of the nacelles occurred at or near the maximum cross-sectional area of the wing-body combination.

2. In the case of the nacelles located at the 40-percent-semispan station, moving the nacelles a moderate amount ahead of and down from the local wing chord caused substantial reductions in transonic interference drag. Further chordwise and vertical movement of the pylon-suspended nacelles did not result in any appreciable drag reductions but had a favorable effect on the drag-break Mach number.

3. At Mach numbers up to about 0.80, the strut and strut-end junctures of the pylon-suspended nacelles appeared to be responsible for a large interference drag.

4. Moderate thickening of the wing root was accomplished without penalty in minimum drag or maximum lift-drag ratio when the nacelles were submerged in the wing root aft of the maximum thickness station.

5. At high Mach numbers the wing-tip nacelles had the lowest incremental drag coefficients and the highest maximum lift-drag-ratio values of the various nacelle configurations investigated on the wing-body configuration with the 6-percent-thick wing.

6. The various solid nacelle configurations reduced the drag-break Mach number of the basic models about 0.020 to 0.040.

7. Generally, the addition of the various nacelles to the basic wing-body configurations produced small increases in the lift-curve-slope characteristics.

8. The pylon-suspended and underslung nacelles produced destabilizing moments whereas the submerged and wing-tip nacelles caused stabilizing moments of the basic model configurations.

Langley Aeronautical Laboratory
     National Advisory Committee for Aeronautics
          Langley Field, Va.

REFERENCES

1. Robinson, Ross B., and Driver, Cornelius: Aerodynamic Characteristics
   at Supersonic Speeds of a Series of Wing-Body Combinations Having
   Cambered Wings With an Aspect Ratio of 3.5 and a Taper Ratio of
   0.2. Effects of Sweep Angle and Thickness Ratio on the Aerodynamic
   Characteristics in Pitch at M = 1.60. NACA RM L51K16a, 1952.

2. Spearman, M. Leroy, and Hilton, John H., Jr.: Aerodynamic Charac-
   teristics at Supersonic Speeds of a Series of Wing-Body Combinations
   Having Cambered Wings With an Aspect Ratio of 3.5 and a Taper Ratio
   of 0.2. Effects of Sweep Angle and Thickness Ratio on the Static
   Lateral Stability Characteristics at M = 1.60. NACA RM L51K15a,
   1952.

3. Hasel, Lowell E., and Sevier, John R., Jr.: Aerodynamic Characteristics
   at Supersonic Speeds of a Series of Wing-Body Combinations Having
   Cambered Wings With an Aspect Ratio of 3.5 and a Taper Ratio of
   0.2. Effect at M = 1.60 of Nacelle Shape and Position on the
   Aerodynamic Characteristics in Pitch of Two Wing-Body Combinations
   With 47° Sweptback Wings. NACA RM L51K14a, 1952.

4. Bielat, Ralph P., Harrison, Daniel E., and Coppolino, Domenic A.:
   An Investigation at Transonic Speeds of the Effects of Thickness
   Ratio and of Thickened Root Sections on the Aerodynamic Charac-
   teristics of Wings With 47° Sweepback, Aspect Ratio 3.5, and Taper
   Ratio 0.2 in the Slotted Test Section of the Langley 8-Foot High-
   Speed Tunnel. NACA RM L51I04a, 1951.

5. Bielat, Ralph P.: A Transonic Wind-Tunnel Investigation of the
   Aerodynamic Characteristics of Three 4-Percent-Thick Wings of
   Sweepback Angles 10.8°, 35°, and 47°, Aspect Ratio 3.5, and Taper
   Ratio 0.2 in Combination With a Body. NACA RM L52B08, 1952.

6. Wright, Ray H., and Ritchie, Virgil S.: Characteristics of a Tran-
   sonic Test Section With Various Slot Shapes in the Langley 8-Foot
   High-Speed Tunnel. NACA RM L51H10, 1951.

7. Osborne, Robert S.: A Transonic-Wing Investigation in the Langley
   8-Foot High-Speed Tunnel at High Subsonic Mach Numbers and at a
   Mach Number of 1.2. Wing-Fuselage Configuration Having a Wing of
   45° Sweepback, Aspect Ratio 4, Taper Ratio 0.6, and NACA 65A006
   Airfoil Section. NACA RM L50H08, 1950.

8. Wright, Ray H., and Ward, Vernon G.: NACA Transonic Wind-Tunnel
   Test Sections. NACA RM L8J06, 1948.

9. DeYoung, John: Theoretical Additional Span Loading Characteristics
    of Wings With Arbitrary Sweep, Aspect Ratio, and Taper Ratio.
    NACA TN 1491, 1947.
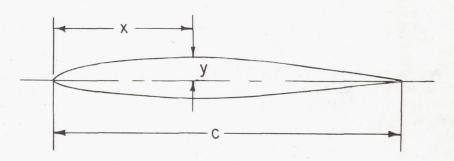
10. Ritchie, Virgil S., and Pearson, Albin O.: Calibration of the Slotted
    Test Section of the Langley 8-Foot Transonic Tunnel and Preliminary
    Experimental Investigation of Boundary-Reflected Disturbances.
    NACA RM L51K14, 1952.

11. Spreeman, Kenneth P., and Alford, William J., Jr.: Investigation of
    the Effects of Geometric Changes in an Underwing Pylon-Suspended
    External-Store Installation on the Aerodynamic Characteristics of
    a 45° Sweptback Wing at High Subsonic Speeds. NACA RM L50L12, 1951.

12. Hoffman, Sherwood, and Pepper, William B., Jr.: Transonic Flight
    Tests to Determine Zero-Lift Drag and Pressure Recovery of Nacelles
    Located at the Wing Tips on a 45° Sweptback Wing and Body Combina-
    tion. NACA RM L51K02, 1952.

13. Whitcomb, Richard T., and Kelly, Thomas C.: A Study of the Flow Over
    a 45° Sweptback Wing-Fuselage Combination at Transonic Mach Numbers.
    NACA RM L52D01, 1952.

14. Pendley, Robert E., and Smith, Norman F.: An Investigation of the
    Characteristics of Three NACA 1-Series Nose Inlets at Subcritical
    and Supercritical Mach Numbers. NACA RM L8L06, 1949.

TABLE I

AIRFOIL COORDINATES FOR THE 6-PERCENT-THICK AND

THICKENED-ROOT WINGS

[Coordinates are in percent of chord]

6-percent-thick wing

x/c	y/c Upper surface	y/c Lower surface
0	0.061	0
.5	.577	.376
.75	.717	.446
1.25	.919	.534
2.5	1.304	.621
5.0	1.872	.761
7.5	2.318	.857
10	2.668	.980
15	3.150	1.269
20	3.482	1.496
25	3.701	1.697
30	3.858	1.846
35	3.946	1.960
40	3.981	2.021
45	3.937	2.030
50	3.823	1.977
55	3.613	1.872
60	3.342	1.697
65	3.018	1.487
70	2.651	1.277
75	2.231	1.059
80	1.785	.849
85	1.339	.639
90	.892	.420
95	.446	.210
100	0	0
L.E. radius = 0.0024c		

Thickened root wing

x/c	Root station y/c Upper surface	Root station y/c Lower surface
0	0.301	0
.5	1.120	.754
.75	1.335	.904
1.25	1.658	1.141
2.5	2.261	1.507
5.0	3.208	2.024
7.5	3.919	2.433
10	4.500	2.799
15	5.362	3.445
20	5.965	3.984
25	6.395	4.414
30	6.718	4.716
35	6.912	4.910
40	6.977	5.017
45	6.912	4.996
50	6.675	4.823
55	6.288	4.522
60	5.771	4.113
65	5.168	3.618
70	4.457	3.101
75	3.725	2.584
80	2.929	2.067
85	2.239	1.550
90	1.486	1.034
95	.732	.517
100	0	0
L.E. radius = 0.0099c		

NACA
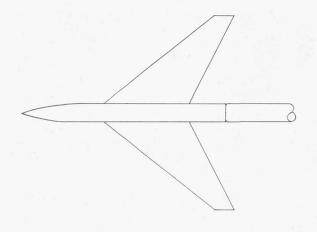
TABLE II

SUMMARY OF AERODYNAMIC CHARACTERISTICS OF VARIOUS NACELLE CONFIGURATIONS ON THE 6-PERCENT-THICK WING MODEL
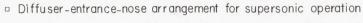
Basic model W_1	C_D				$\left(\dfrac{L}{D}\right)_{max}$		M_B		Aerodynamic-center location, percent $\bar{c}$	
	$C_L=0$		$C_L=0.3$				$C_L=$ 0	$C_L=$ 0.3		
	M=0.70	1.10	.70	1.10	.70	1.10			.70	1.10
	0.0095	0.0223	0.0167	0.0333	19.2	9.0	0.975	0.957	36.5	50.6

Nacelle position	ΔC_D				$\left(\dfrac{L}{D}\right)_{max}$		M_B		Aerodynamic-center location, percent $\bar{c}$	
	$C_L=0$		$C_L=0.3$				$C_L=$ 0	$C_L=$ 0.3		
	M=0.70	1.10	.70	1.10	.70	1.10			.70	1.10
N_1 $x/\bar{c}=0.800$ $z/\bar{c}=0.166$	0.0035	0.0138	0.0063	0.0167	13.2	6.4	0.950	0.920	33.0	47.1
N_2 $x/\bar{c}=1.181$ $z/\bar{c}=0.267$	.0033	.0087	.0033	.0101	15.2	7.3	.938	.925	33.0	47.6
N_3 $x/\bar{c}=1.562$ $z/\bar{c}=0.362$	.0035	.0084	.0036	.0102	15.1	7.3	.970	.950	33.0	48.5
N_{2a} $x/\bar{c}=0.768$ $z/\bar{c}=0.267$	.0036	.0097	.0033	.0107	14.9	7.0	.950	.920	32.5	47.3
N_u	.0015	.0137	.0033	.0162	15.0	6.4	.950	.932	34.0	49.0
N_{wt}	.0022	.0064	.0033	.0067	15.5	7.9	.950	.928	43.0	56.3
N_{s1}	.0010	.0087	.0033	.0092	15.3	7.3	.950	.933	37.8	55.3

○ Diffuser-entrance-nose arrangement for subsonic operation
□ Diffuser-entrance-nose arrangement for supersonic operation
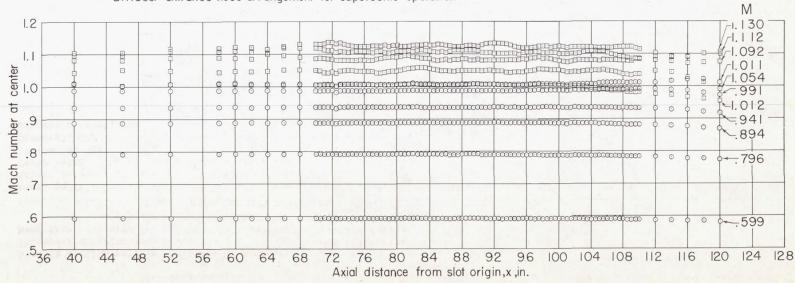
Figure 1.- Mach number distributions along the center of the test section.

Wing Details

Airfoil section parallel to plane of symmetry
Thickness distribution . . . . NACA 65A series
Mean line ordinates . . . 1/3 of NACA 230 series + NACA 6-series
uniform-load mean line (a = 1.0) for
a design lift coefficient of 0.1

Area, sq ft 1.143
Aspect ratio 3.5
Taper ratio 0.2
Incidence, deg 0
Dihedral, deg 0
Geometric twist, deg 0
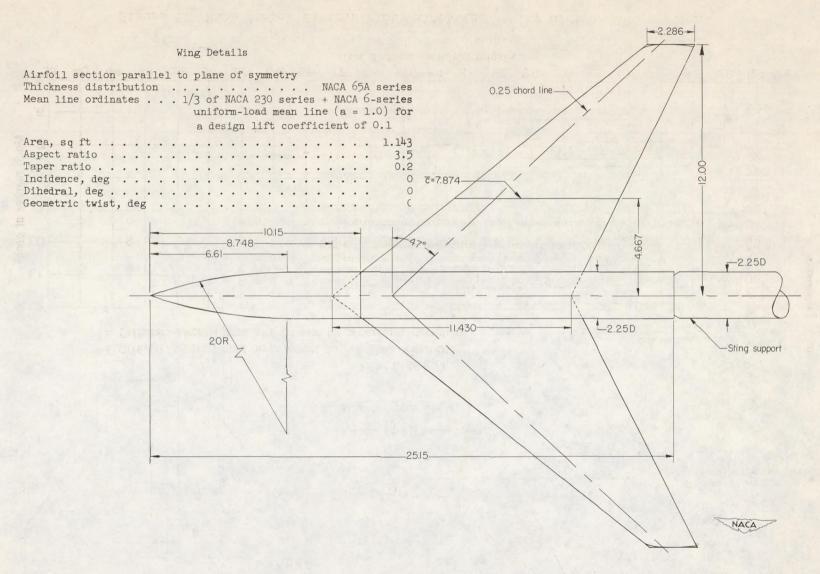
Figure 2.- Model plan form. All dimensions are in inches.

4.667

$\overline{c}$ = 7.874

Coordinates for nacelle nose
and afterbody

X	r
0	0.005
1.00	.287
1.50	.422
2.00	.536
2.50	.626
3.00	.693
3.50	.735
4.00	.750

Nose radius = 0.005 inch

Nacelle position	$\frac{x}{c}$	$\frac{z}{c}$
N_1	0.800	0.166
N_2	1.181	.267
N_3	1.562	.362
N_u*	.540	.095

*Note: Upper surface of underslung nacelles (N_u) is tangent to wing-chord plane.

47°

x

5.00

A — A
Strut section
NACA 65A005

16°

75°

A

A

16°

r

1.50

r

X

4.00

6.27

X

4.00

z

.40 b/2

NACA
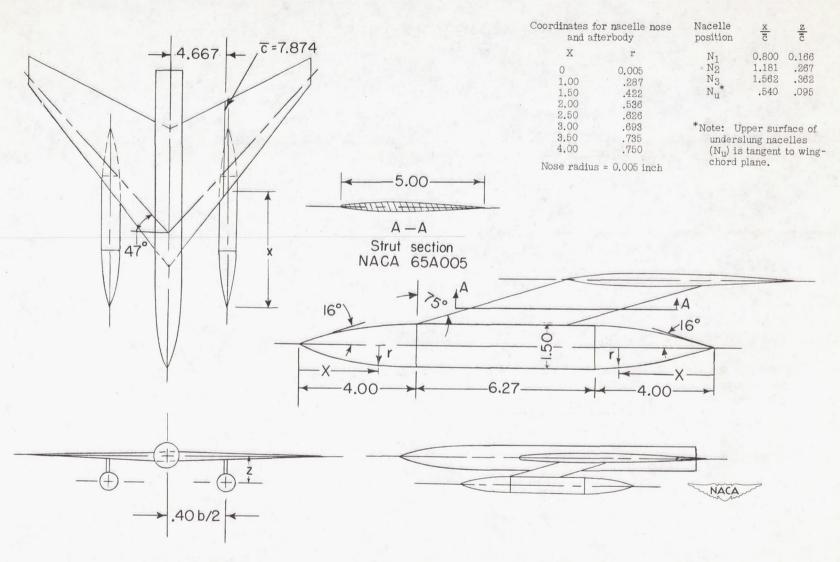
Figure 3.- Location of underslung and pylon-suspended nacelles on the
6-percent-thick wing-body configuration. All dimensions are in
inches.
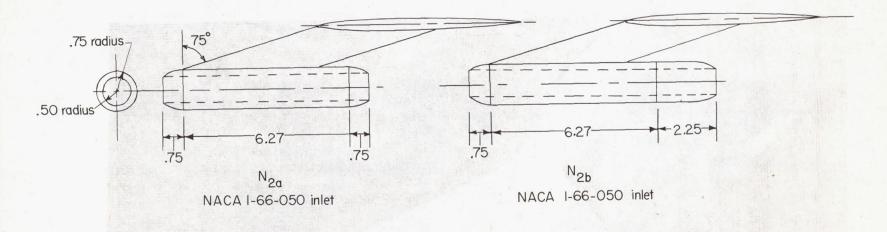
(a) View from front.

(b) View from rear.

Figure 4.- Pylon-suspended nacelles in position N_2 installed on the 6-percent-thick wing-body configuration. Ducted nacelle N_{2a} mounted on the left wing and faired nacelle mounted on right wing.

.75 radius

.50 radius

75°

.75

6.27

.75

N_{2a}

NACA 1-66-050 inlet

.75

6.27

2.25

N_{2b}

NACA 1-66-050 inlet

2.25

6.27

.75

N_{2c}

NACA 1-66-050 inlet

2.25

6.27

.75

N_{2d}

NACA 1-66-100 inlet

NACA
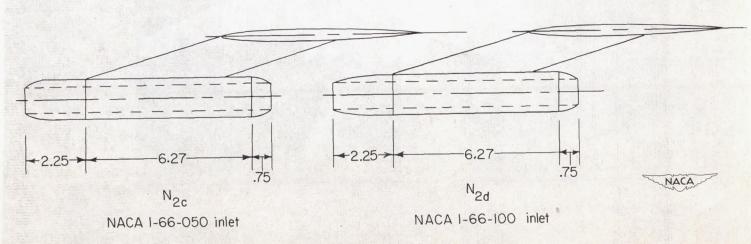
Figure 5.- Ducted nacelles investigated in position 2 on 6-percent-thick wing-body configuration.
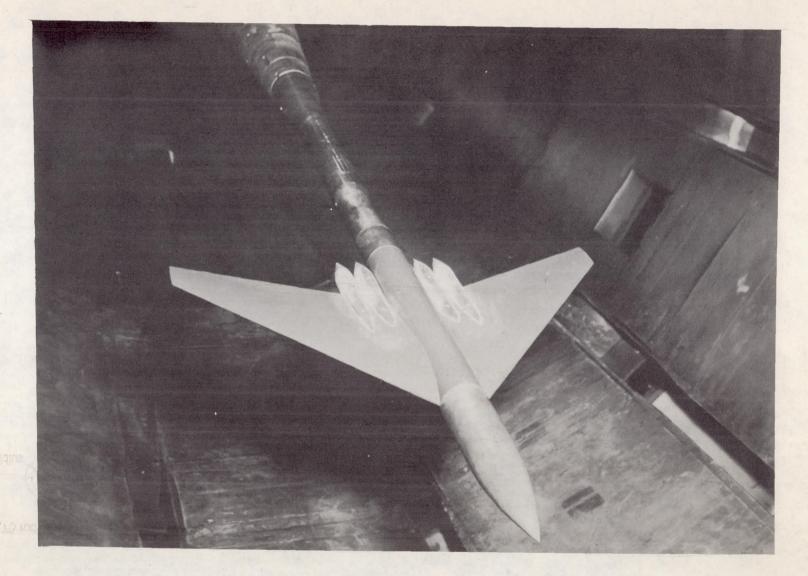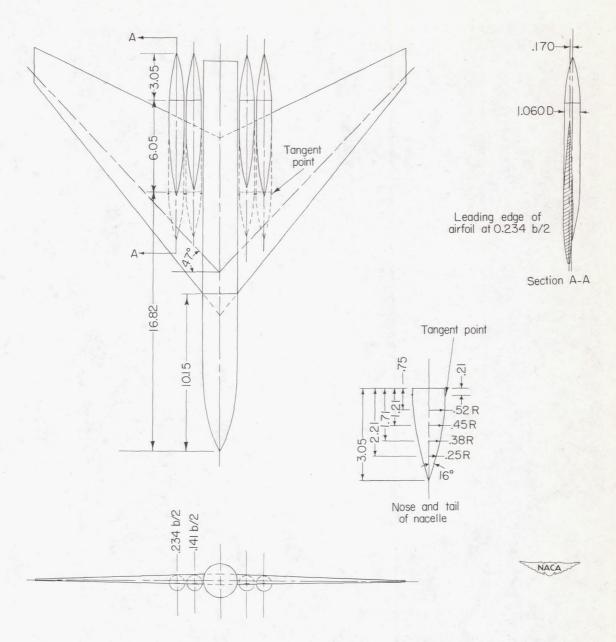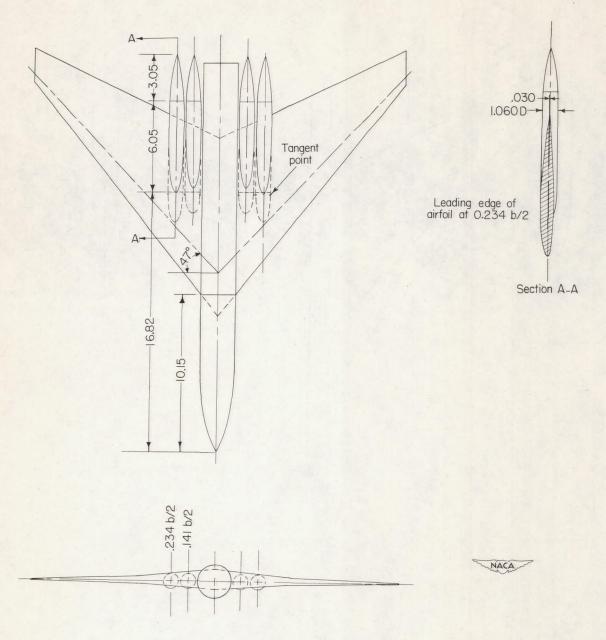
Figure 6.- Submerged nacelles installed on the thickened-root wing-body configuration.

L-71806

A ←

3.05

6.05

Tangent
point

A ←

47°

16.82

10.15

.170 →

1.060 D →

Leading edge of
airfoil at 0.234 b/2

Section A-A

Tangent point

.75

.21

3.05

2.21

1.7

1.21

.52 R

.45 R

.38 R

.25 R

16°

Nose and tail
of nacelle

.234 b/2

.141 b/2

NACA

(a) N_{sl} on 6-percent-thick wing.

Figure 7.- Locations and details of the submerged nacelles on the wing-
body configuration. All dimensions are in inches.

.030
1.060 D

Leading edge of
airfoil at 0.234 b/2

Section A-A

A

3.05

6.05

Tangent
point

A

47°

16.82

10.15

.234 b/2
.141 b/2

NACA

(b) N_{s2} on thickened-root wing.

Figure 7.- Concluded.
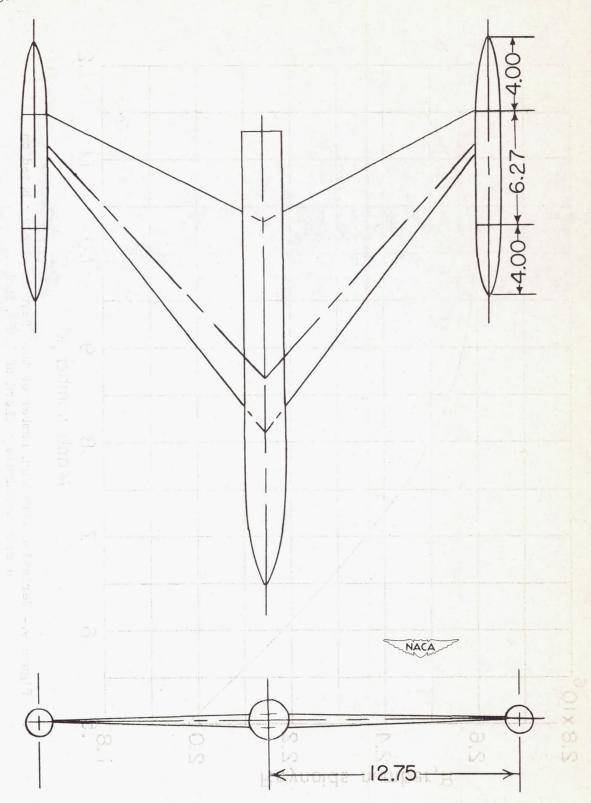
Figure 8.- Location of wing-tip nacelles on the 6-percent-thick wing-
body configuration. All dimensions are in inches.
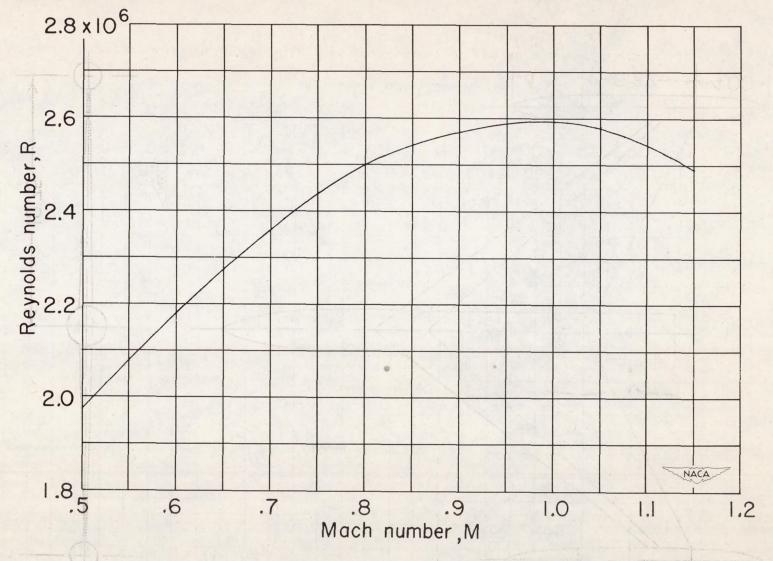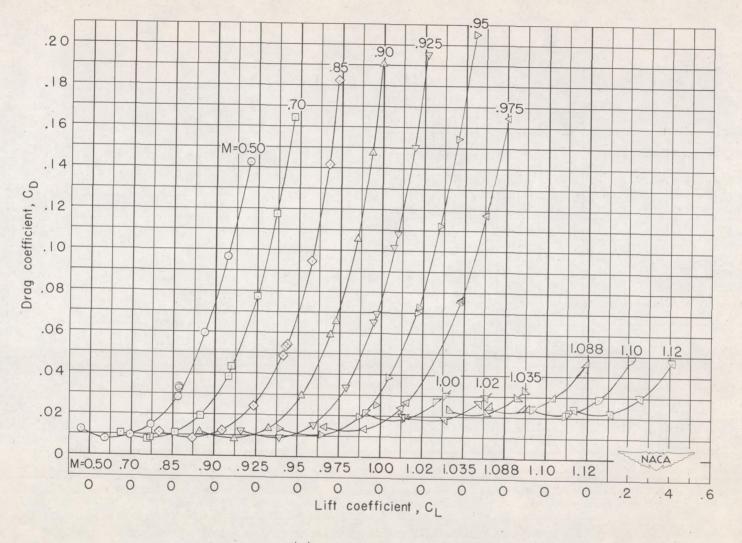
Figure 9.- Variation with Mach number of test Reynolds number based on a mean aerodynamic chord of 7.874 inches.
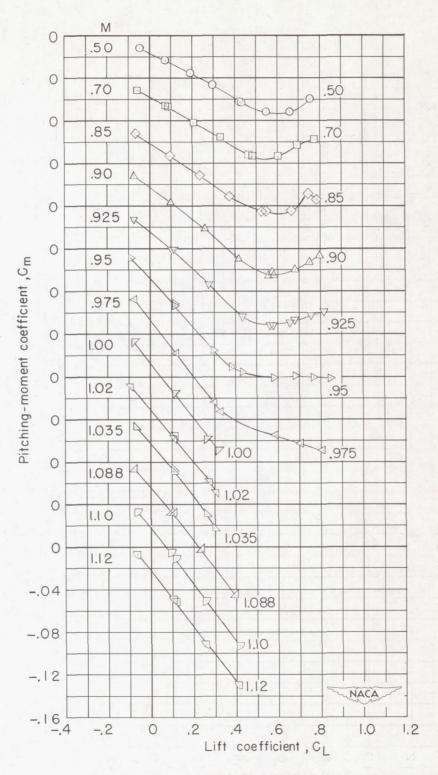
(a) Angle of attack.

Figure 10.- Variation with lift coefficient of the aerodynamic charac-
teristics for the 6-percent-thick wing. W_1.
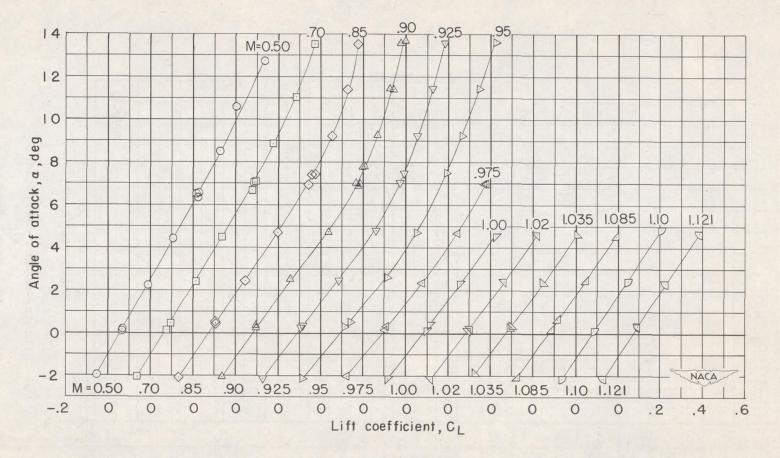
(b) Drag coefficient.

Figure 10.- Continued.
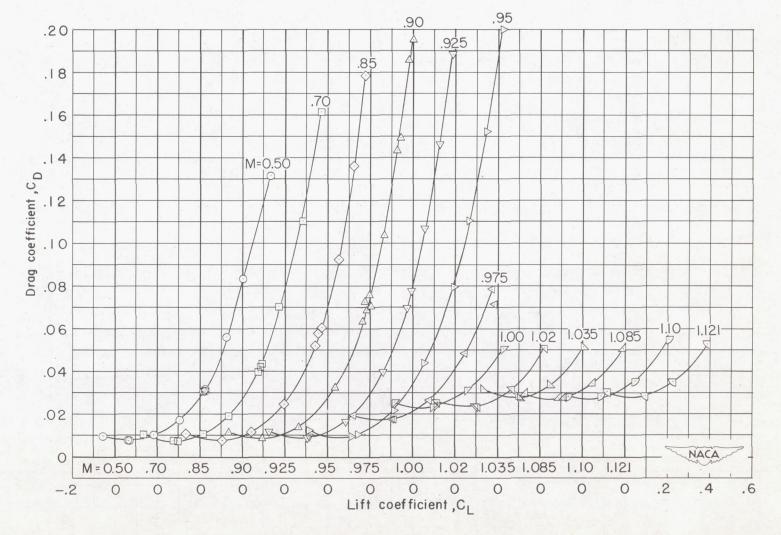
(c)   Pitching-moment coefficient.

Figure 10.- Concluded.
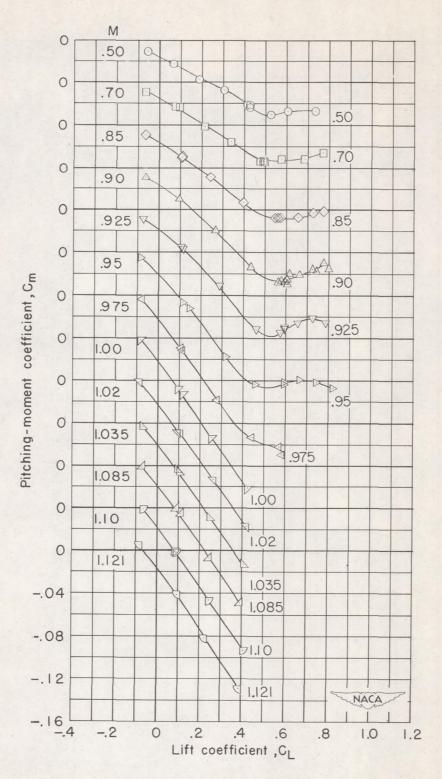
(a) Angle of attack.

Figure 11.- Variation with lift coefficient of the aerodynamic charac-
teristics for the thickened-root wing W_2.

(b) Drag coefficient.
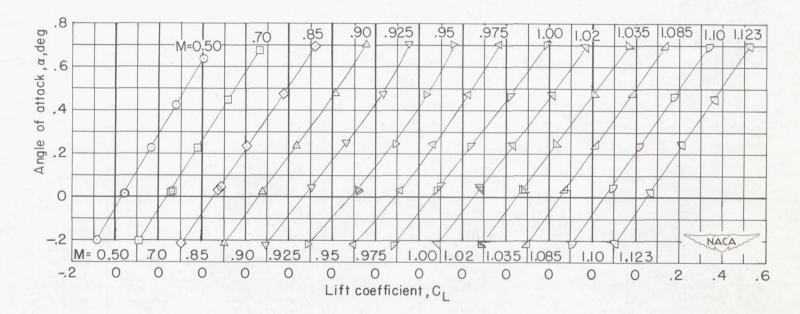
Figure 11.- Continued.

(c) Pitching-moment coefficient.

Figure 11.- Concluded.

.8

.6

.4

Angle of attack, α, deg

.2

0

−.2

M=0.50   .70   .85   .90   .925   .95   .975   1.00   1.02   1.035   1.085   1.10   1.123

M= 0.50   .70   .85   .90   .925   .95   .975   1.00   1.02   1.035   1.085   1.10   1.123

−.2   0   0   0   0   0   0   0   0   0   0   0   0   .2   .4   .6

NACA

Lift coefficient, C_L
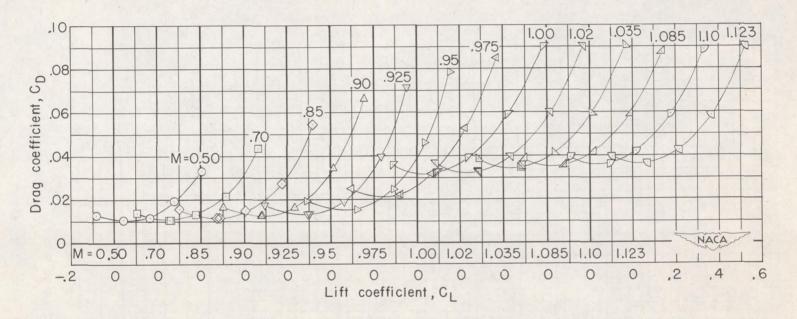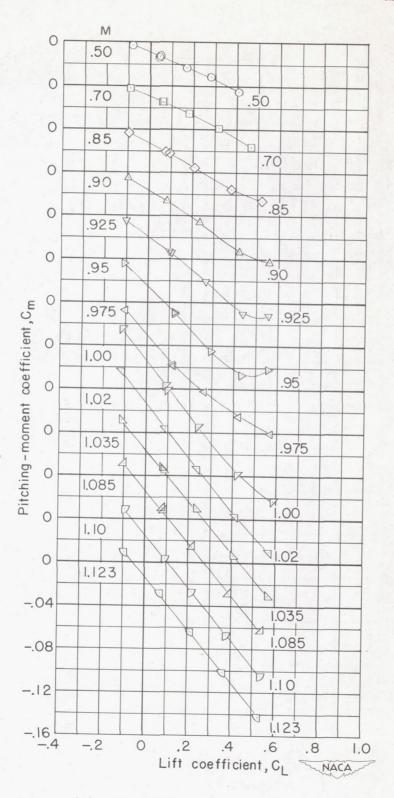
(a) Angle of attack.

Figure 12.- Variation with lift coefficient of the aerodynamic charac-
teristics for wing 1, with underslung nacelles N_u.
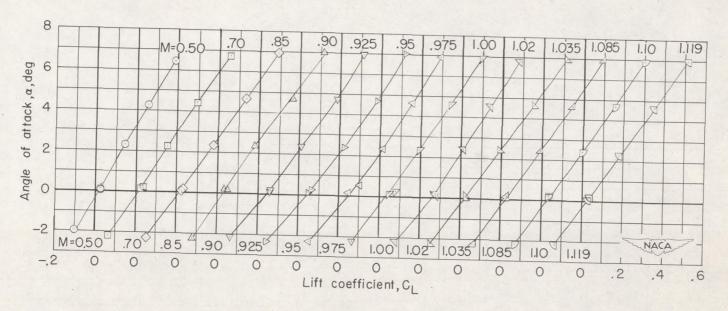
(b) Drag coefficient.

Figure 12.- Continued.
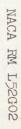
(c) Pitching-moment coefficient.
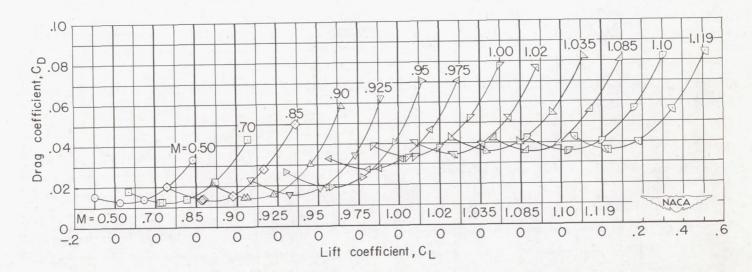
Figure 12.- Concluded.

(a) Angle of attack.
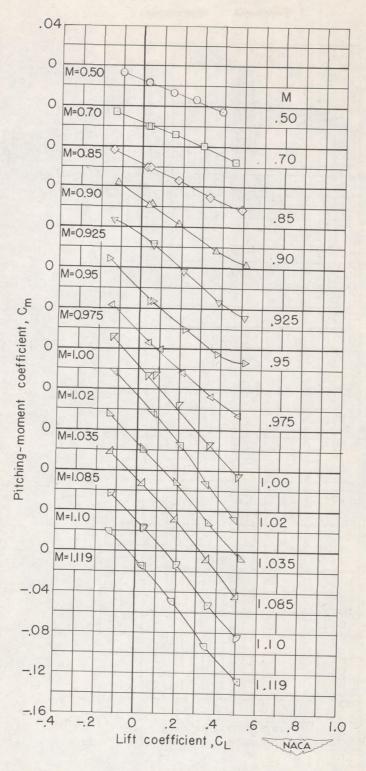
Figure 13.- Variation with lift coefficient of the aerodynamic characteristics for wing 1, with pylon-suspended nacelles, position N_1.
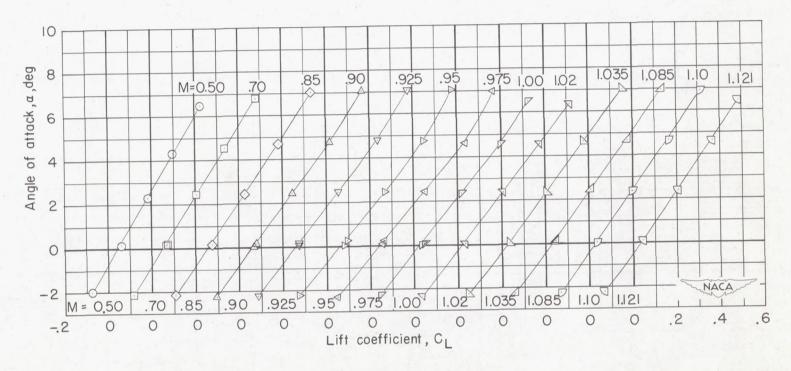
(b) Drag coefficient.

Figure 13.- Continued.
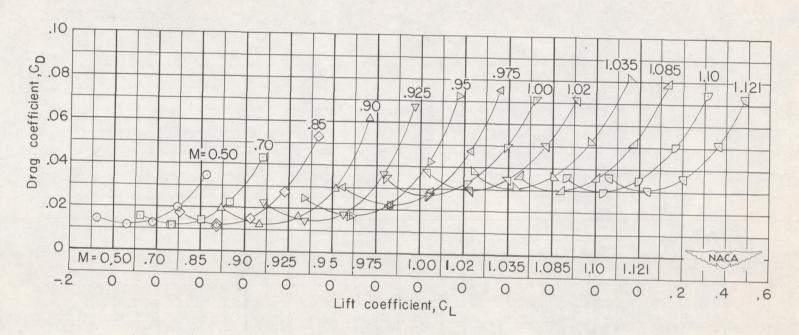
(c) Pitching-moment coefficient.

Figure 13.- Concluded.
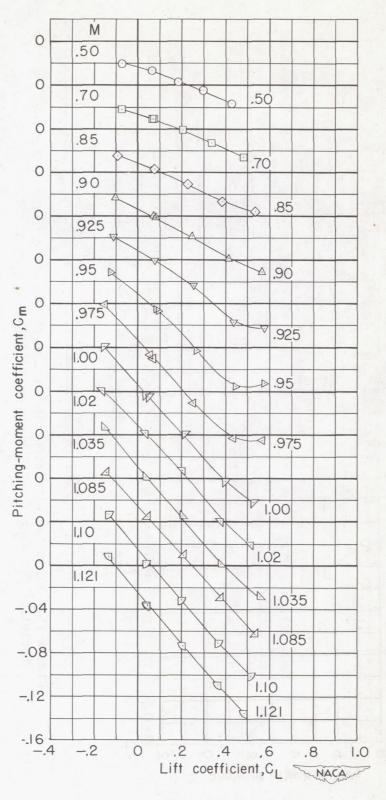
(a) Angle of attack.

Figure 14.- Variation with lift coefficient of the aerodynamic charac-
teristics for wing 1, with pylon-suspended nacelles, position N_2.
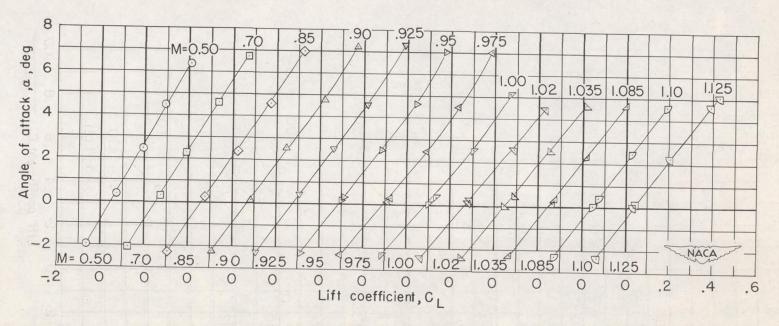
(b) Drag coefficient.

Figure 14.- Continued.
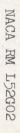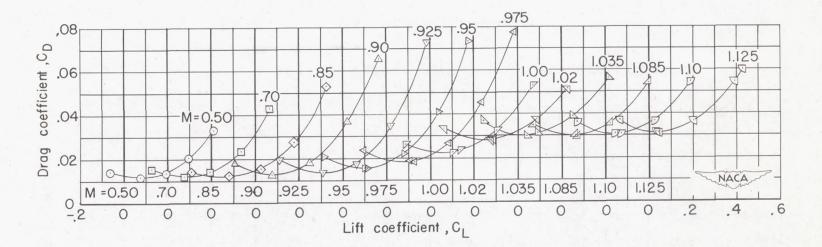
(c) Pitching-moment coefficient.

Figure 14.- Concluded.

(a) Angle of attack.
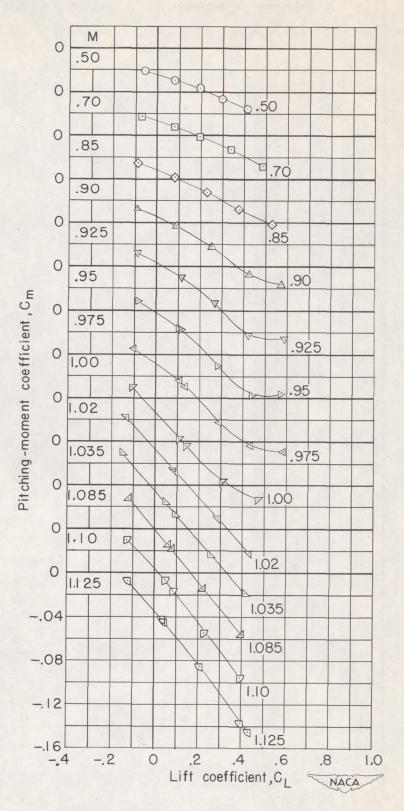
Figure 15.- Variation with lift coefficient of the aerodynamic charac-
teristics for wing 1, with pylon-suspended nacelles, position N_3.
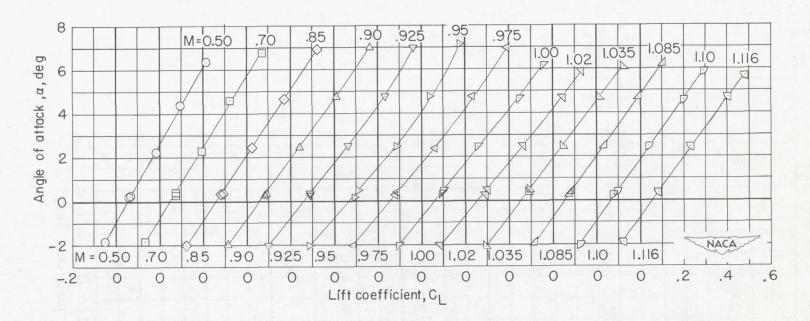
(b) Drag coefficient.

Figure 15.- Continued.
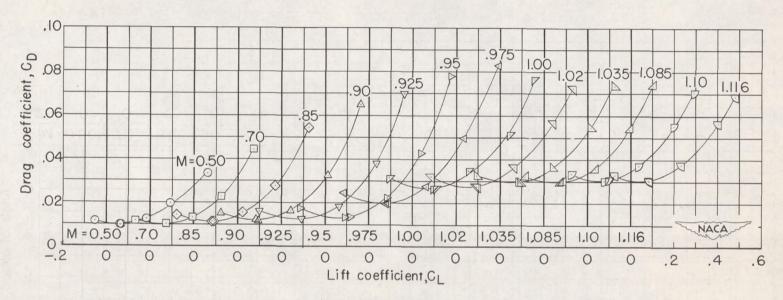
(c) Pitching-moment coefficient.

Figure 15.- Concluded.
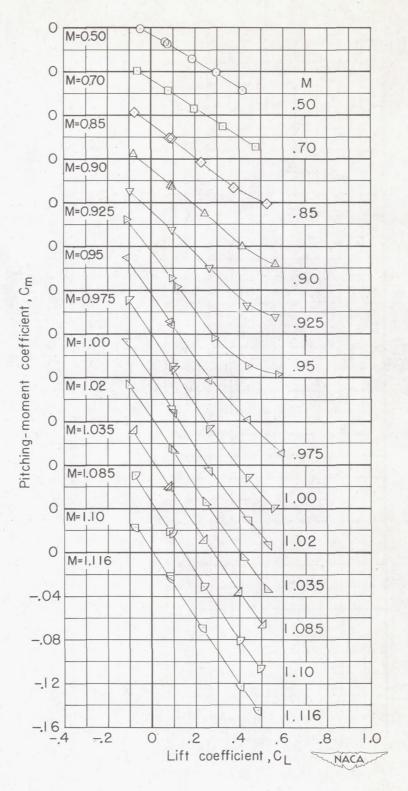
(a) Angle of attack.

Figure 16.- Variation with lift coefficient of the aerodynamic characteristics for wing 1, with submerged nacelles N_{s1}.
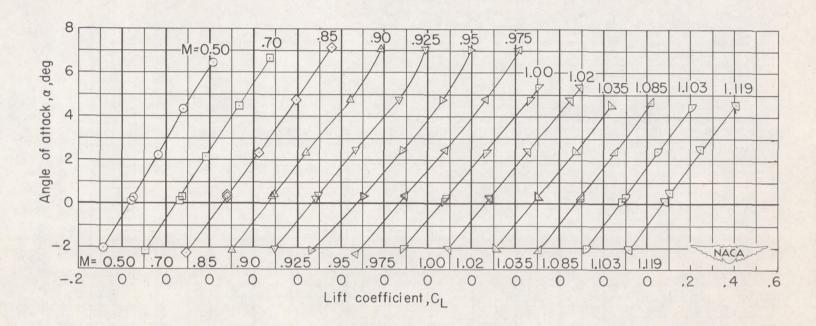
(b) Drag coefficient.

Figure 16.- Continued.
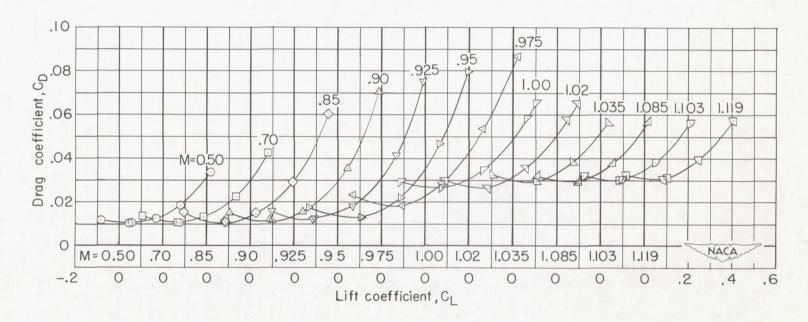
(c) Pitching-moment coefficient.

Figure 16.- Concluded.

(a) Angle of attack.
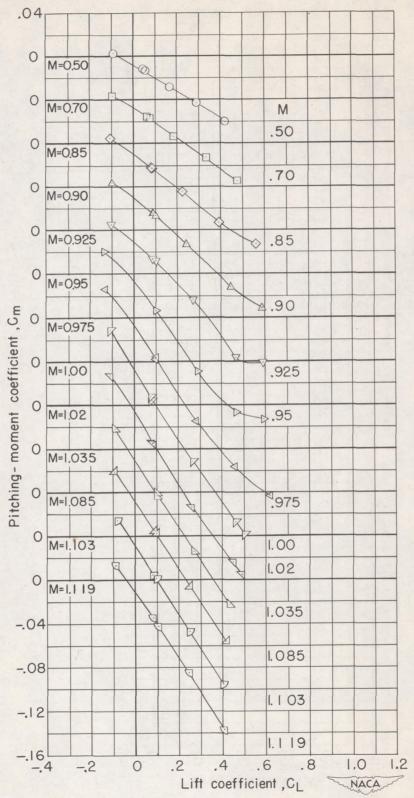
Figure 17.- Variation with lift coefficient of the aerodynamic charac-
teristics for wing 2, with submerged nacelles N_{s2}.

(b) Drag coefficient.
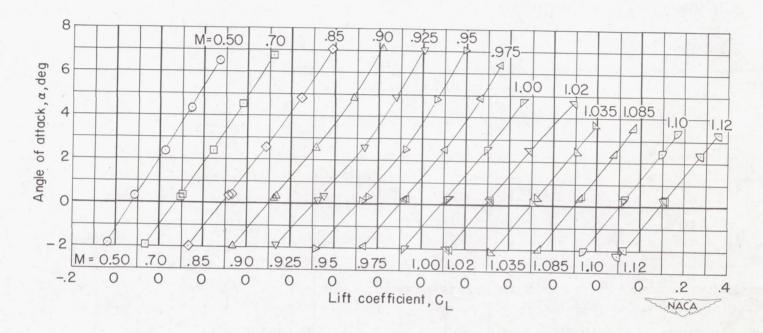
Figure 17.- Continued.

(c) Pitching-moment coefficient.
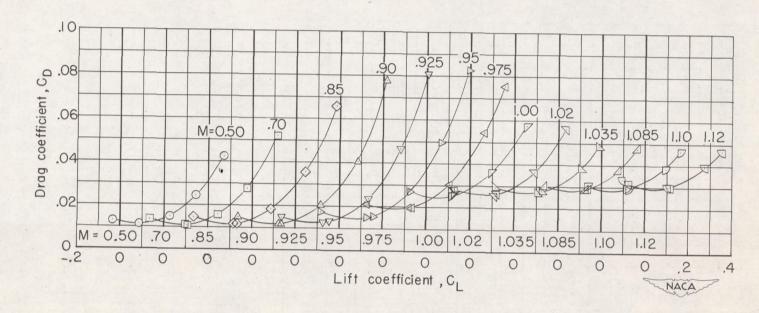
Figure 17.- Concluded.
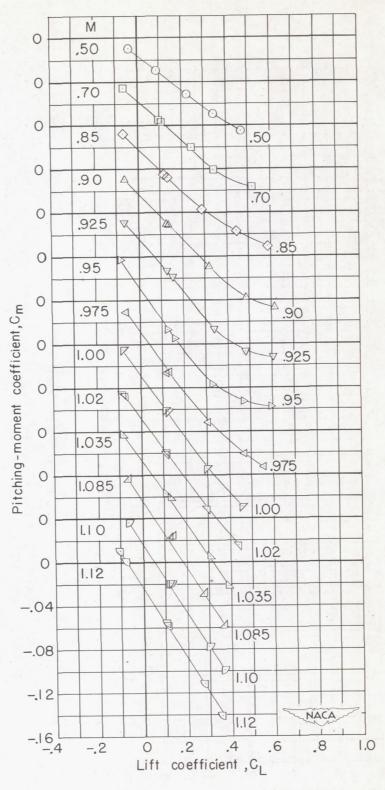
(a) Angle of attack.

Figure 18.- Variation with lift coefficient of the aerodynamic characteristics for wing 1, with wing-tip nacelles N_{wt}.
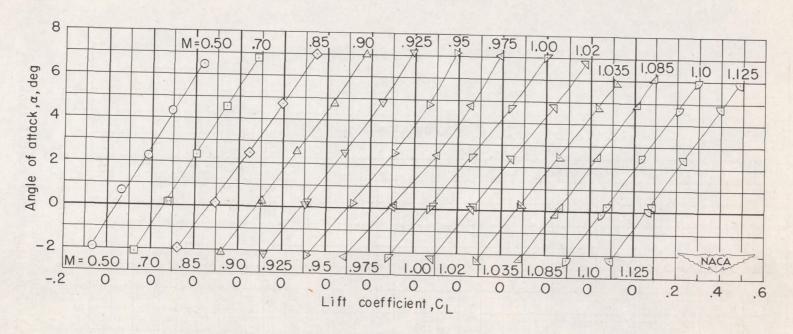
(b) Drag coefficient.

Figure 18.- Continued.
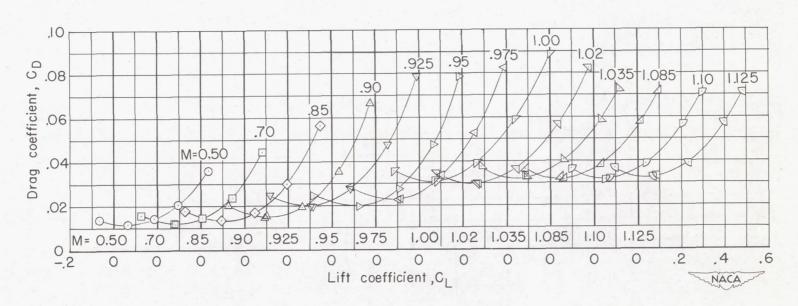
(c) Pitching-moment coefficient.

Figure 18.- Concluded.

(a) Angle of attack.
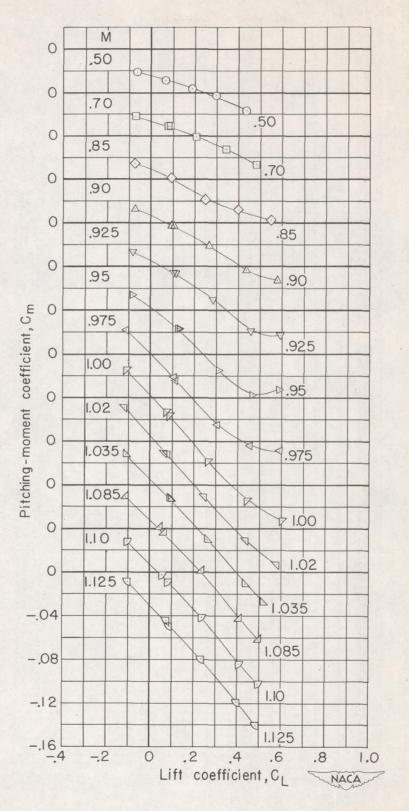
Figure 19.- Variation with lift coefficient of the aerodynamic charac-
teristics for wing 1, with pylon-suspended nacelles at position N_2,
modification a (with air flow). N_{2a}.
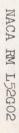
(b) Drag coefficient.
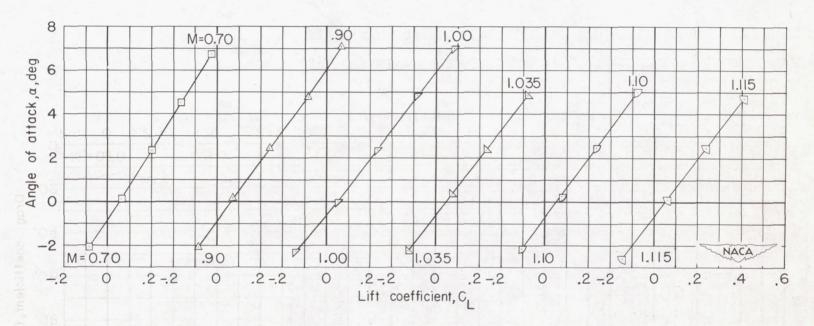
Figure 19.- Continued.

(c) Pitching-moment coefficient.
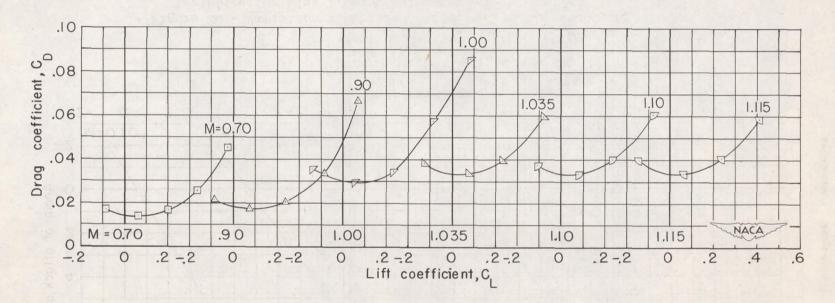
Figure 19.- Concluded.
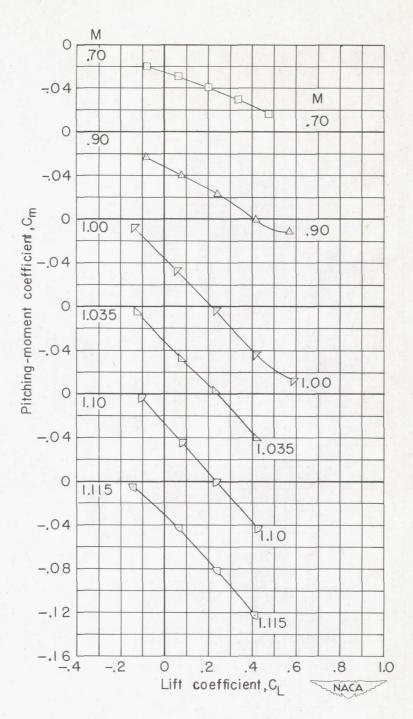
(a) Angle of attack.

Figure 20.- Variation with lift coefficient of the aerodynamic charac-
teristics for wing 1, with pylon-suspended nacelles, position N_2,
modification b (with air flow). N_{2b}.
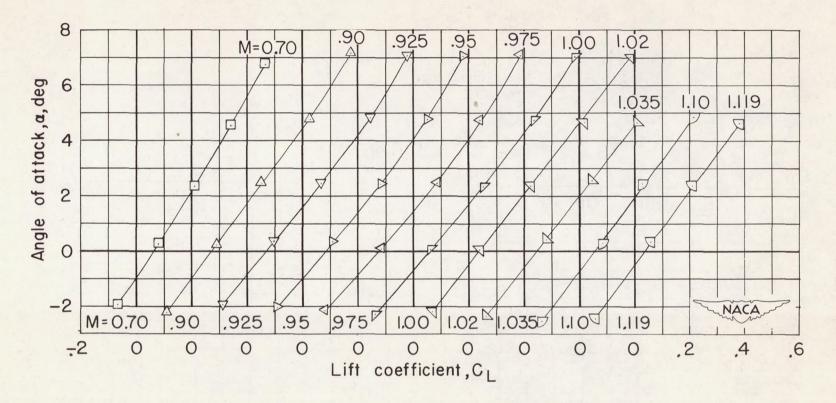
(b) Drag coefficient.

Figure 20.- Continued.
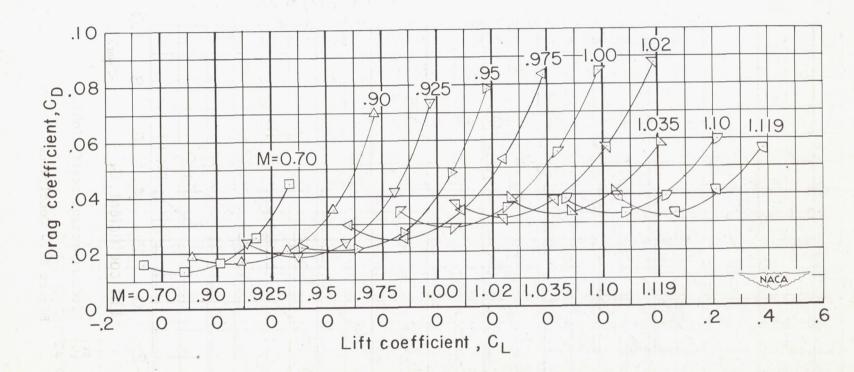
(c)   Pitching-moment coefficient.

Figure 20.- Concluded.
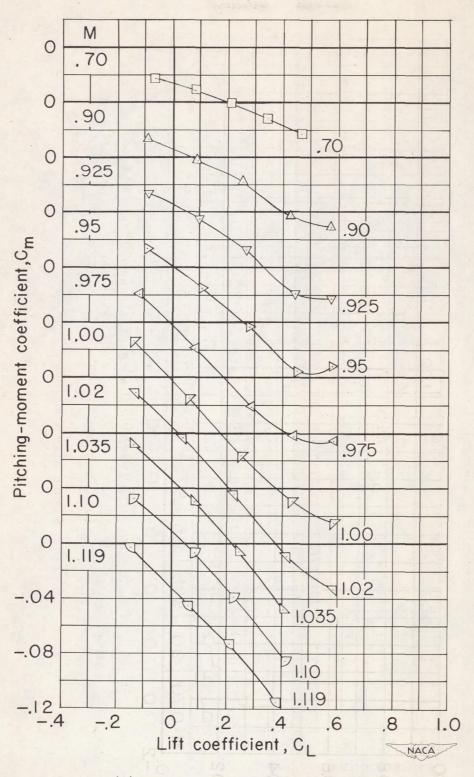
(a) Angle of attack.

Figure 21.- Variation with lift coefficient of the aerodynamic charac-
teristics for wing 1, with pylon-suspended nacelles, position N_2,
modification c (with air flow). N_{2c}.

(b) Drag coefficient.

Figure 21.- Continued.

(c) Pitching-moment coefficient.

Figure 21.- Concluded.

(a) Angle of attack.
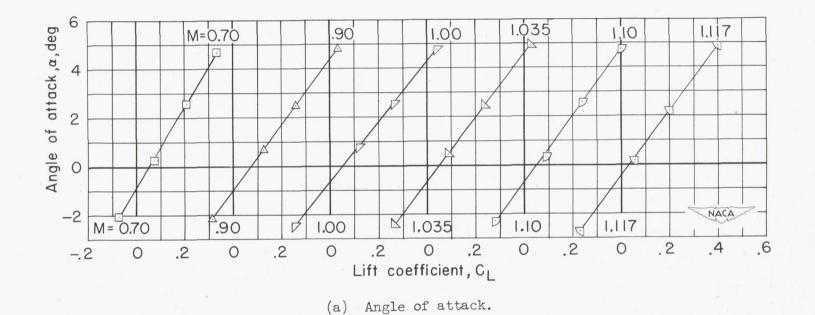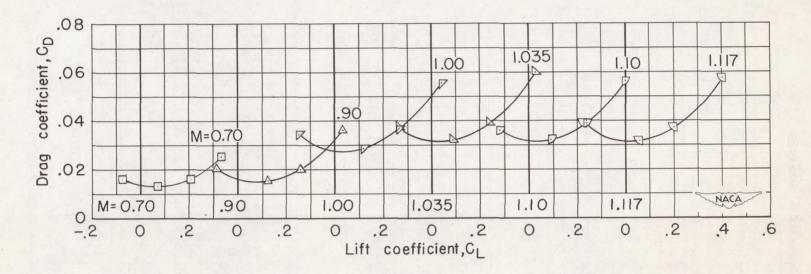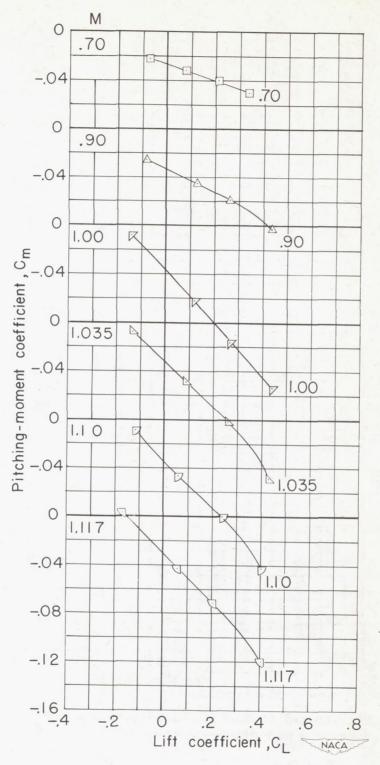
Figure 22.- Variation with lift coefficient of the aerodynamic charac-
teristics for wing 1, with pylon-suspended nacelles, position N_2,
modification d (with air flow). N_{2d}.

(b) Drag coefficient.

Figure 22.- Continued.

(c) Pitching-moment coefficient.

Figure 22.- Concluded.
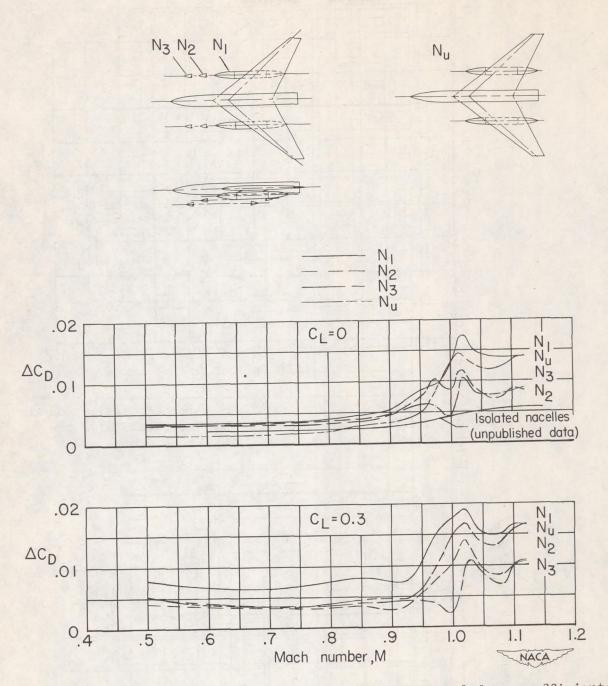
Figure 23.- Variation with Mach number of the incremental drag coefficients for the underslung and pylon-suspended nacelles. 6-percent-thick wing.
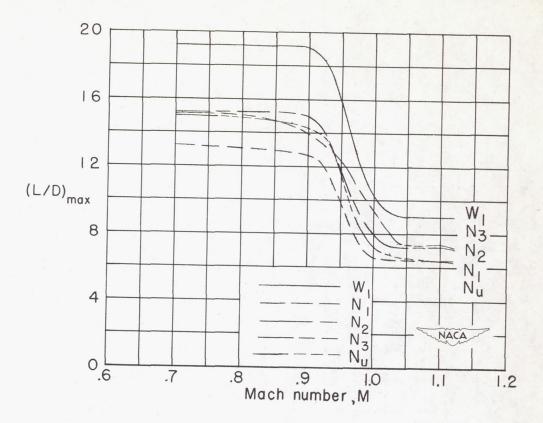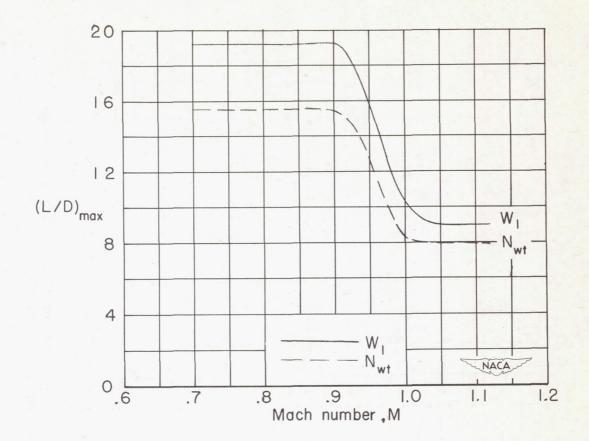
Figure 24.- Effect of underslung and pylon-suspended nacelles on the variation of maximum lift-drag ratio with Mach number for the 6-percent-thick wing-body configuration.
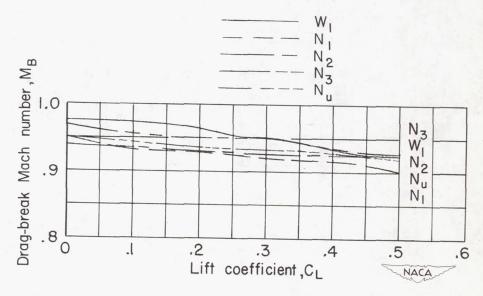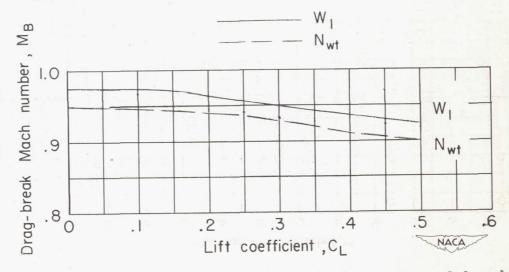

Figure 25.- Effect of underslung and pylon-suspended nacelles on the variation of the drag-break Mach number with lift coefficient for the 6-percent-thick wing-body configuration.
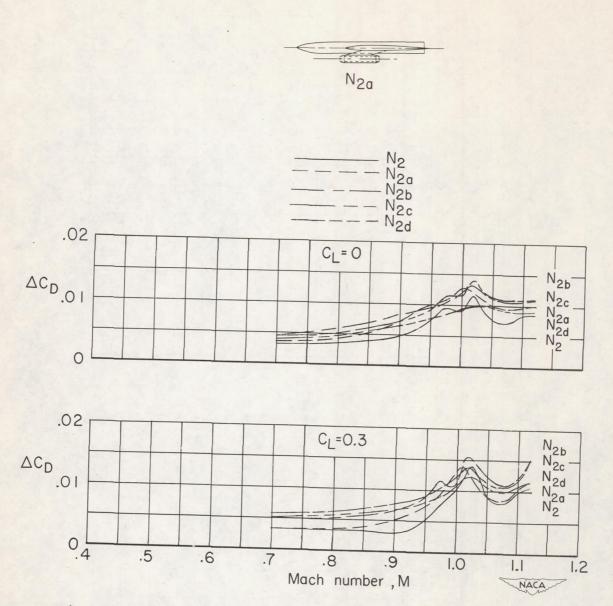
Figure 26.- Variation with Mach number of the incremental drag coefficients for the pylon-suspended nacelles with air flow. 6-percent-thick wing.
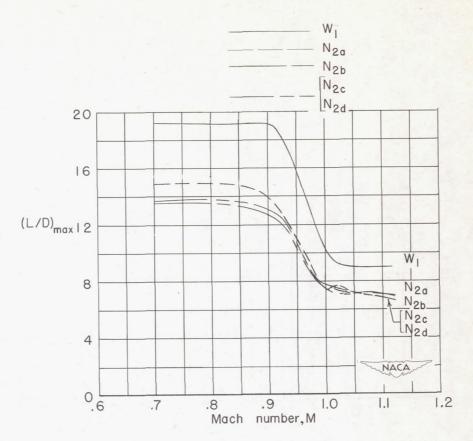
Figure 27.- Effect of pylon-suspended nacelles with air flow on the variation of maximum lift-drag ratio with Mach number for the 6-percent-thick wing-body configuration.
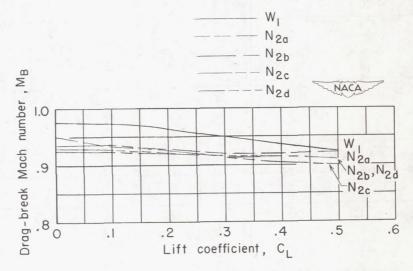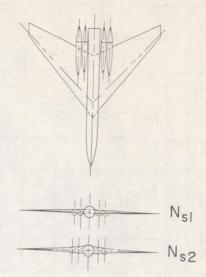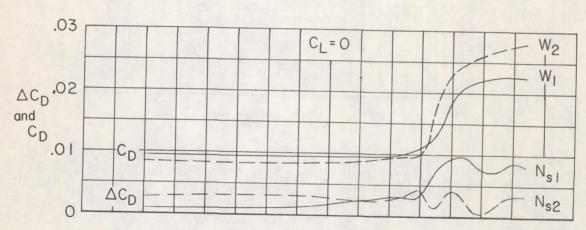
Figure 28.- Effect of pylon-suspended nacelles with air flow on the variation of drag-break Mach number with lift coefficient for the 6-percent-thick wing-body configuration.
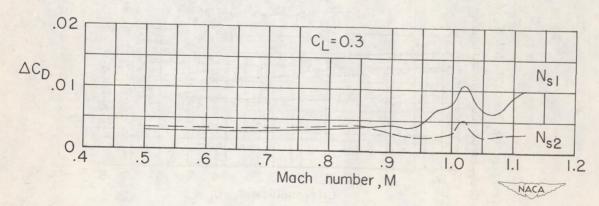
Figure 29.- Variation with Mach number of the incremental drag coefficients for the submerged nacelles. 6-percent-thick and thickened-root wings.
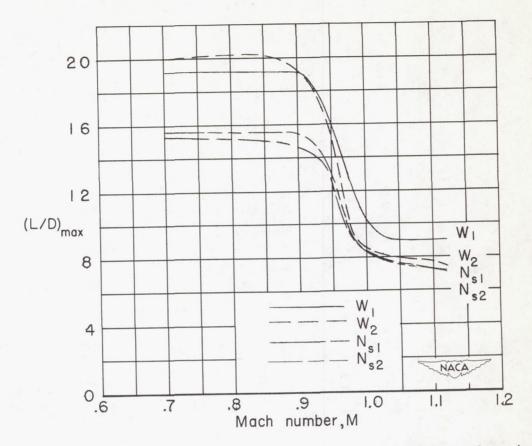
Figure 30.- Effect of submerged nacelles on the variation of maximum lift-drag ratio with Mach number for the 6-percent-thick and the thickened-root wing-body configurations.
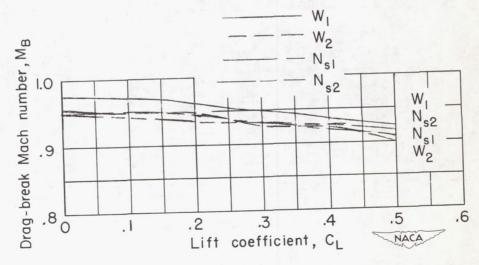
Figure 31.- Effect of submerged nacelles on the variation of drag-break Mach number with lift coefficient for the 6-percent-thick and the thickened-root wing-body configurations.
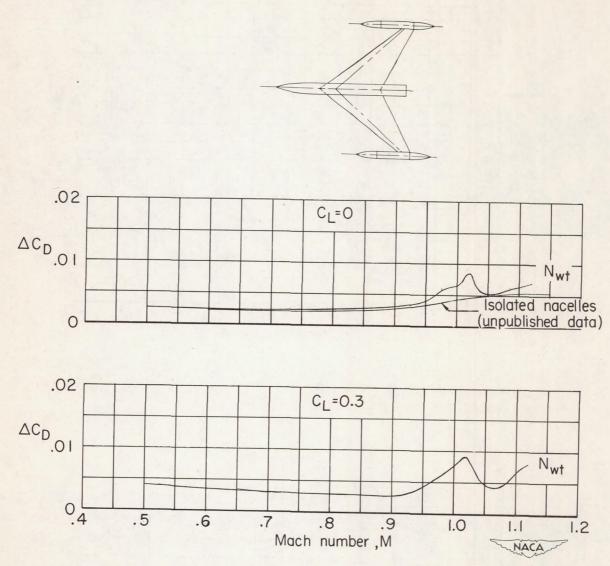
Figure 32.- Variation with Mach number of the incremental drag coefficients for the wing-tip nacelles. 6-percent-thick wing.

Figure 33.- Effect of wing-tip nacelles on the variation of maximum lift-drag ratio with Mach number for the 6-percent-thick wing-body configuration.

Figure 34.- Effect of wing-tip nacelles on the variation of drag-break Mach number with lift coefficient for the 6-percent-thick wing-body configuration.
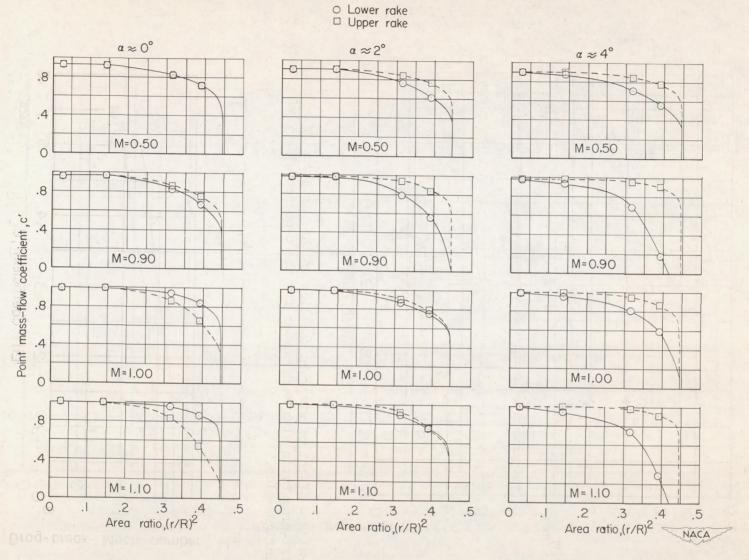
Figure 35.- Variation of point-mass flow coefficient with area ratio for the pylon-suspended nacelle N_{2a}.
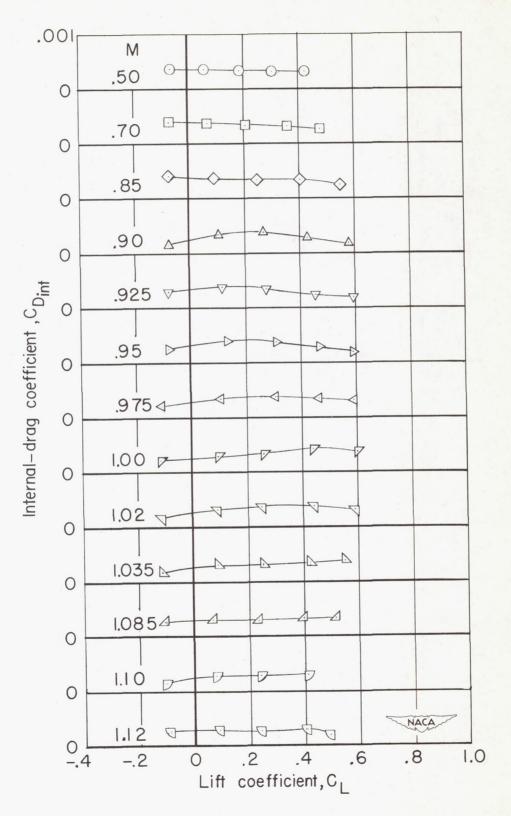
Figure 36.- Variation of internal-drag coefficient with lift coefficient
for pylon-suspended nacelle N_{2a}.
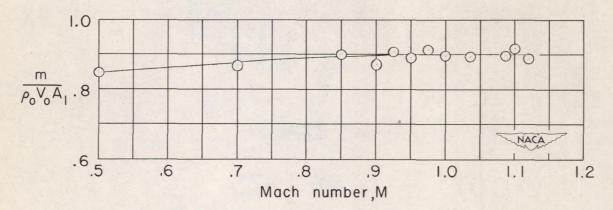
Figure 37.- Variation of the mass-flow ratio with Mach number for the pylon-suspended nacelles. N_{2a}. $\alpha = 0°$.
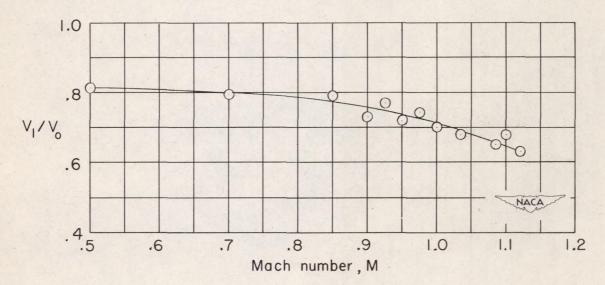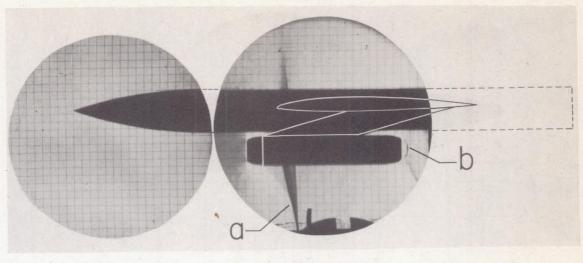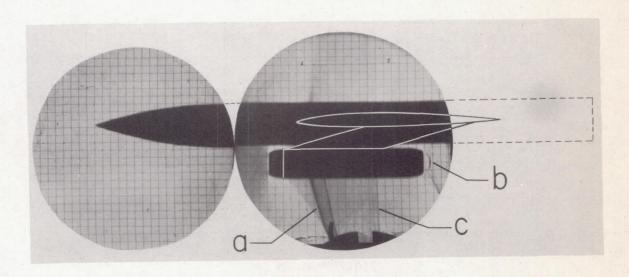
Figure 38.- Variation of inlet velocity with Mach number for the pylon-suspended nacelles N_{2a}. $\alpha = 0°$.

M=0.97   M=0.975
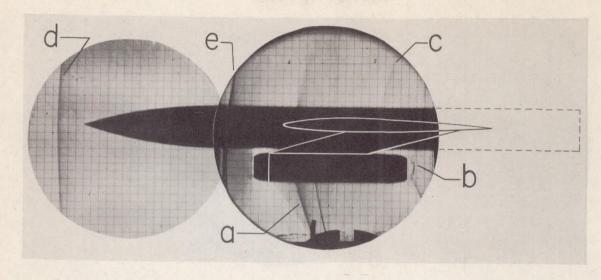
M=0.99   M=1.00
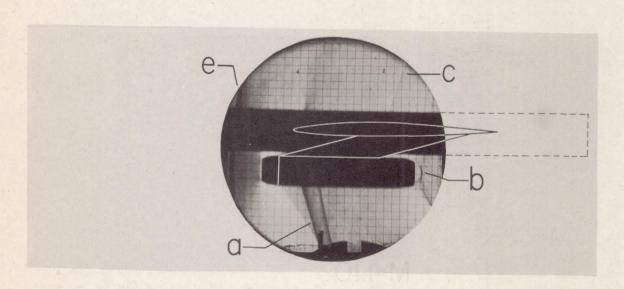
Figure 39.- Schlieren photographs of the flow for the wing-body
    configuration with pylon-suspended nacelles N_{2a}. $\alpha = 0^o$.
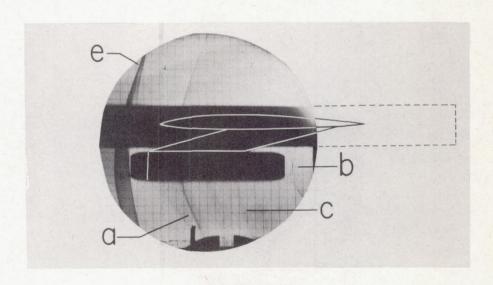
L-75150

M=1.024   M=1.020

M=1.035

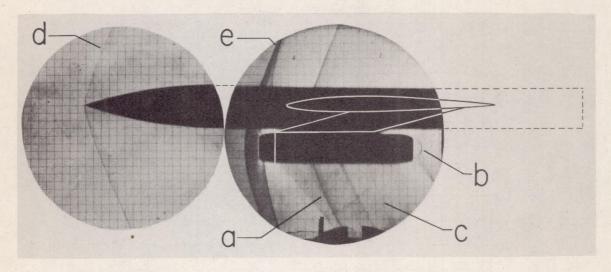Figure 39.- Continued.
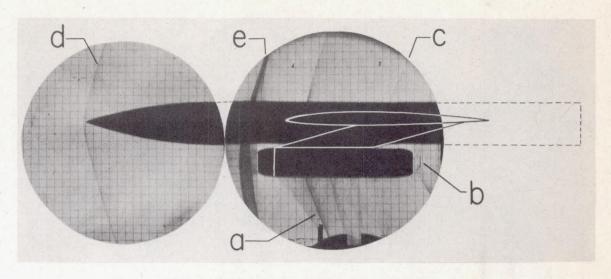
M=1.088   M=1.085

M=1.10

Figure 39.- Continued.

M=1.113   M=1.125

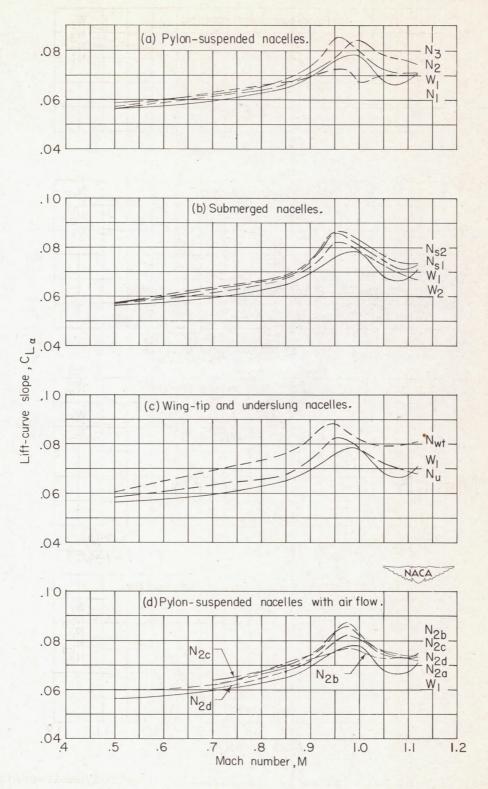Figure 39.- Concluded.

L-75153

Figure 40.- Effect of nacelles on the variation of lift-curve slope with Mach number for the 6-percent-thick wing-body configuration and the thickened-root wing-body configuration.
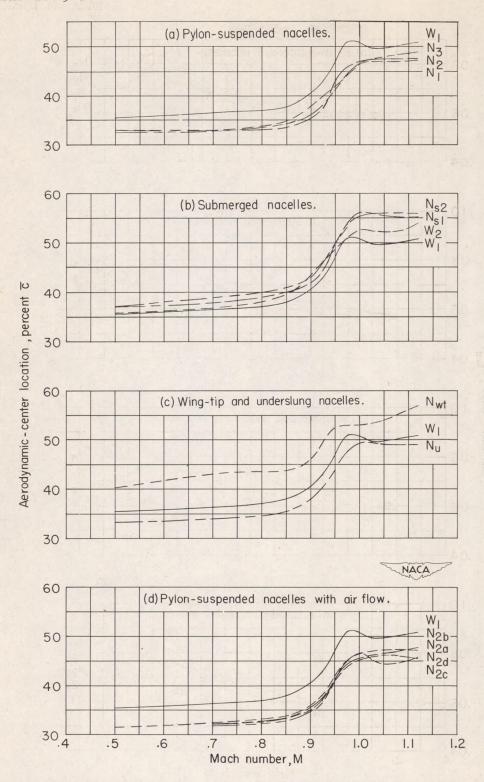
Figure 41.- Effect of nacelles on the variation of aerodynamic-center location with Mach number for the 6-percent-thick wing-body configuration and the thickened-root wing-body configuration.